SANDIA REPORT

SAND99–0681
Unlimited Release
Printed April 1999

Hydrogen Production for Fuel Cells by Selective Dehydrogenation of Alkanes in Catalytic Membrane Reactors

Timothy J. Gardner, Elaine P. Boespflug, C. Jeffrey Brinker, Allen G. Sault, Andy C. Y. Tsai, and John P. Collins

Prepared by
Sandia National Laboratories
Albuquerque, New Mexico 87185 and Livermore, California 94550

Sandia is a multiprogram laboratory operated by Sandia Corporation, a Lockheed Martin Company, for the United States Department of Energy under Contract DE-AC04-94AL85000.

Sandia National Laboratories

Issued by Sandia National Laboratories, operated for the United States Department of Energy by Sandia Corporation.

Available to DOE and DOE contractors from
Office of Scientific and Technical Information
P.O. Box 62
Oak Ridge, TN 37831

Prices available from (703) 605-6000
Web site: http://www.ntis.gov/ordering.htm

Available to the public from
National Technical Information Service
U.S. Department of Commerce
5285 Port Royal Rd
Springfield, VA 22161

NTIS price codes
Printed copy: A04
Microfiche copy: A01

SAND 99-0681
Unlimited Release
Printed April 1999

Hydrogen Production for Fuel Cells by Selective Dehydrogenation of Alkanes in Catalytic Membrane Reactors

Timothy J. Gardner and Allen G. Sault
New Materials and Validation Department

Elaine P. Boespflug
Explosive Materials/Subsystems Department

C. Jeffrey Brinker
Direct Fabrication Technologies Department

Sandia National Laboratories
P.O. Box 5800
Albuquerque, NM 87185-0710

Andy C. Y. Tsai
Advanced Materials Laboratory
University of New Mexico
Albuquerque, NM 87131

John P. Collins
Amoco Research Center
Napierville, IL 60563

Abstract

Hydrogen-powered polymer electrolyte membrane (PEM) fuel cells, fueled by on-board H_2 generation from liquid fuels, represent a potential enabling technology for future vehicles. Much current effort has been devoted to the use of steam reforming or partial oxidation of liquid fuels for on-board H_2 generation, but these technologies generate large amounts of CO, which can poison PEM fuel cells. The purpose of this project was to develop a catalytic membrane reactor system for the generation of pure H_2 *via* selective dehydrogenation of liquid fuels. Separation of hydrogen from hydrocarbons was to be achieved by modification of commercial asymmetric alumina membrane tubes with permselective microporous ceramic membranes. Hydrous titanium oxide (HTO) and silica-doped hydrous titanium oxide (HTO:Si) ion exchange materials were evaluated as a component of the microporous ceramic composite membrane material and as a support for bulk dehydrogenation catalysts,

respectively. Finally, experiments were performed using a bulk dehydrogenation catalyst in conjunction with a microporous ceramic membrane to demonstrate a proof of concept for H_2 generation by n-heptane dehydrogenation/dehydrocyclization using a catalytic membrane reactor. This scheme offers a potential method for increasing hydrogen production rates without increasing reactor size by overcoming equilibrium limitations on conversion, an important consideration for transportation applications or for remote electricity generation for civilian or military applications.

Acknowledgment

The authors thank United Catalysts, Inc. for stimulating technical discussions and for providing samples of commercial dehydrogenation catalysts. The efforts of Tim Boyle in preparing organometallic tin precursors for use in Pt-Sn catalyst preparation, as well as the overall catalyst preparation and characterization efforts of Linda McLaughlin, are gratefully acknowledged. This work was supported by the United States Department of Energy under Contract DE-AC04-94AL85000. Sandia is a multiprogram laboratory operated by Sandia Corporation, a Lockheed Martin Company, for the United States Department of Energy. This report summarizes activities performed under the laboratory directed research and development program at Sandia National Laboratories (project number 96-0396).

Contents

Figures

Tables

Hydrogen Production for Fuel Cells by Selective Dehydrogenation of Alkanes in Catalytic Membrane Reactors

Introduction

The need for increased energy efficiency and decreased environmental emissions provides a strong driving force for research into alternatives to the internal combustion engine for transportation needs. One promising alternate technology is electricity-generating fuel cells [1-3]. Pure H_2 fuel for these systems is very compatible with the current polymer electrolyte membrane (PEM) technology [1-3]. However, safely storing hydrogen with energy densities sufficient to provide adequate vehicle range currently represents an important obstacle to the successful utilization of H_2-powered fuel cells [4]. A potential solution to this difficulty involves on-board generation of H_2 from liquid fuels, thereby solving fuel storage problems and simultaneously taking advantage of the existing infrastructure for distribution of liquid fuels. For hybrid vehicles [5,6], on-board H_2 generation would allow the same liquid fuel to be used to power both an internal combustion engine and a fuel cell, thereby avoiding weight and space penalties associated with separate fuel storage systems. A wide range of chemical processes (primarily steam reforming and partial oxidation) have been proposed for on-board reforming of various liquid fuels (gasoline, diesel fuel, methanol, etc.) to produce H_2 for PEM fuel-cell powered vehicles [4,7-11]. The focus of this project was the development of a catalytic dehydrogenation membrane reactor to generate H_2 from liquid hydrocarbons (alkanes) and simultaneously separate the H_2 from the olefin coproducts.

The selective dehydrogenation scheme we propose also provides advantages over steam reforming, another prospective on-board H_2 production scheme. On-board steam reforming requires extensive water management that is absent with dehydrogenation. Dehydrogenation therefore avoids the weight and space penalty associated with the need to pump, store, and recycle water for steam reforming. Steam reforming also generates substantial amounts of CO and CO_2, which wastes a large fraction of the available energy content of the fuel. The presence of CO represents a serious problem since it has a significant poisoning effect on PEM fuel cells if it is not rigorously removed. In addition to H_2, selective dehydrogenation generates only hydrocarbons (olefins) that are easier to separate from H_2 than CO and CO_2, that are not severe poisons for PEM fuel cells, and that can be collected and reused as fuel for an internal combustion engine or to generate heat to drive the endothermic dehydrogenation reaction.

Steam reforming is also endothermic, requiring large heat input, so the endothermic nature of dehydrogenation is not necessarily a disadvantage relative to reforming. Offsetting the important advantages of dehydrogenation is the fact that steam reforming recovers virtually all of the hydrogen in the fuel as H_2, while in dehydrogenation a substantial fraction of the hydrogen remains in the dehydrogenated products. Thus, a dehydrogenation unit will likely require a larger throughput than a steam reforming unit to produce comparable amounts of H_2. We believe that other advantages offered by dehydrogenation more than offset this disadvantage, with the net result being a smaller and more efficient on-board H_2 generation unit. While partial oxidation

reactions are exothermic in nature, such reactions are difficult to control such that CO and H_2 are selectively produced without the formation of combustion by-products (CO_2 and H_2O). A conceptual on-board H_2 generation/fuel cell system is illustrated below in Figure 1.

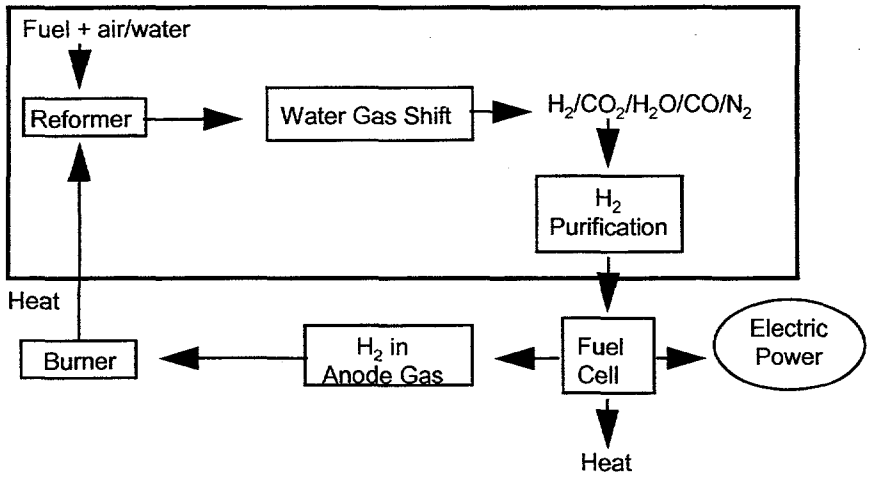

Figure 1. Conceptual on-board H_2 generation/fuel cell system (after ref. [4]). The large box encompassing the reforming, water gas shift, and H_2 purification steps represents that portion of an on-board H_2 generation/fuel cell system which could potentially be replaced by a catalytic membrane reactor. The reformer process unit shown could utilize either a partial oxidation or a steam reforming reaction for H_2 generation.

Many authors have provided reviews of catalytic membrane reactors, pointing out their potential advantages and current limitations [12-20]. Since many chemical reactions are reversible in nature (e.g., hydrogenation/dehydrogenation), conversions which can be achieved to produce a given product slate are equilibrium limited. However, catalytic membrane reactors that combine selective separation (i.e., permselectivity) of a given product species with the chemical reaction can lead to increased reactant conversion to the desired products. Likewise, potentially unfavorable secondary reactions involving product species can be limited by selective product species removal. Other possible advantages are related to increased catalyst life, simplified downstream separation and recovery operations, overall energy savings, and increased safety through control of reactant feed in difficult-to-control reactions (e.g., regulation of O_2 addition for oxidative dehydrogenation versus uncontrolled combustion).

In the case of on-board reforming for H_2 generation, the advantage related to simplified downstream separation and recovery operations is a significant one. It is well known that more conventional steam reforming or partial oxidation of hydrocarbon feeds will produce PEM fuel cell feedstocks that require significant H_2 purification. Figure 1 shows that a number of separate chemical processes are required for CO removal, including both low and high temperature water-gas shift ($CO + H_2O \Leftrightarrow H_2 + CO_2$) [9,21], and additional H_2 purification (e.g., preferential oxidation [PROX] of CO in the presence of H_2) [9-11,22-24]. CO concentrations need to be reduced from nominally 1 % (molar or volume basis) in the post-water gas shift stream to < 40

ppm (< 10 ppm is desirable) in the final fuel cell feedstock to avoid detrimentally affecting fuel cell performance [1, 25]. The use of a membrane with high permselectivity to H_2 (H_2/CO separation factor > 1000) could greatly simplify the overall process for H_2 generation and purification by replacing these additional chemical process units, as well as simultaneously removing other potential contaminant species from the PEM fuel cell feedstock. As illustrated by the large box in Figure 1, a catalytic membrane reactor system could replace the reformer unit, water-gas shift unit(s), and additional H_2 purification (PROX) unit.

In particular, the application of permselective membranes for stand-alone H_2 purification [12-20,26-45] or catalytic membrane reactors in which H_2 generation reactions (dehydrogenation, reforming, etc.) are utilized [12-20,46-61] has recently received considerable interest. The attributes and fundamental mechanisms involved in gas separation using permselective dense metal (Pd) [12-20], polymeric [30,31], or microporous ceramic [32-39] (including zeolites [40-45]) membranes have been reviewed in detail elsewhere. Microporous ceramic membranes, with the combined attributes of low cost and high temperature (> 200°C) stability, relative to Pd membranes and polymeric membranes, respectively, show enormous potential for future catalytic membrane reactor or membrane separation applications. Finally, the combination of catalysis and separation functionalities within a single system also offers a unique opportunity to minimize weight and volume requirements for chemical processes, which is of premier importance in automotive applications. This background indicated that catalytic membrane reactors utilizing microporous ceramic membranes might well be an enabling technology for on-board generation of H_2 for PEM fuel-cell powered vehicles. A schematic illustration of the catalytic membrane reactor concept for alkane dehydrogenation is shown below in Figure 2.

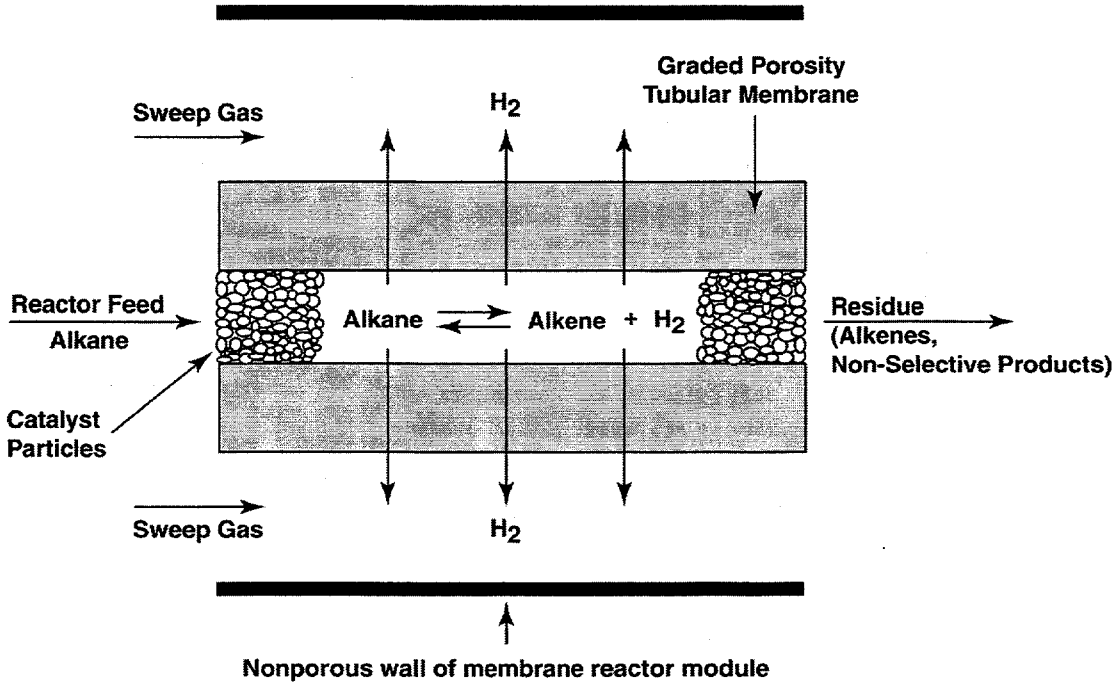

Figure 2. Catalytic membrane reactor concept for selective dehydrogenation of alkanes. The packed catalyst bed would completely occupy the annular space inside the tubular membrane (not shown for simplicity).

The catalyst/membrane system employed in our studies is based upon commercially-available asymmetric alumina membrane tubes with 5 nm average pore diameters [62], modified with a microporous ceramic membrane (made up of one or more deposited layers of various materials) that imparts high H_2 selectivity and permeability. Hydrous titanium oxide (HTO)- or silica-doped hydrous titanium oxide (HTO:Si)-supported Fe and Cr catalysts have demonstrated substantial activity for both ethylbenzene and isobutane dehydrogenation and are likely candidates for other alkane dehydrogenation reactions [63,64]. Part of our studies focus on the evaluation of bulk HTO:Si-supported catalysts in packed catalyst beds tested in a stand-alone mode or in conjunction with microporous ceramic membranes. The former tests will be referred to as conventional packed bed reactor experiments, while the latter tests will be referred to as catalytic membrane reactor experiments.

In addition to high catalyst activity in bulk catalyst applications (conventional packed bed reactors), HTO- or HTO:Si-supported catalyst materials can provide a distinct advantage over commercial dehydrogenation catalysts in that they can be cast as thin films on virtually any substrate [65,66]. Our planned approach was to first modify a commercial asymmetric alumina membrane tube (non-hydrogen selective) with a baseline microporous silica layer. In addition to evaluating these membrane materials in baseline silica form, composite microporous ceramic materials were also evaluated. In previous studies, several materials have been evaluated in the composite membranes as separate layers deposited onto the baseline silica membrane, including silica (an additional layer with different sol chemistry and/or deposition conditions) and titania [34,67]. For this study, as an alternative to titania, a composite membrane was fabricated by depositing a nanocrystalline, ion-exchangeable HTO or HTO:Si layer on top of the baseline silica membrane surface. This approach utilized the underlying baseline silica membrane layer to mediate the delivery of water for hydrolysis and condensation reactions to an alkali titanate precursor layer. The use of the HTO or HTO:Si coatings offers the advantage of allowing a proven catalytic function to be incorporated into the membrane. We anticipated that the intimate association of the membrane and catalyst obtained with this approach would result in improved conversions relative to conventional membrane reactor schemes that use only a bulk catalyst (packed bed) inside the membrane tube. Furthermore, this composite coating approach is amenable to coating low cost, high surface area to volume ratio ceramic monoliths that would be ideal supports for automotive fuel cell applications. A schematic illustration of the graded porosity asymmetric tubular membrane (see Figure 2) is shown in Figure 3.

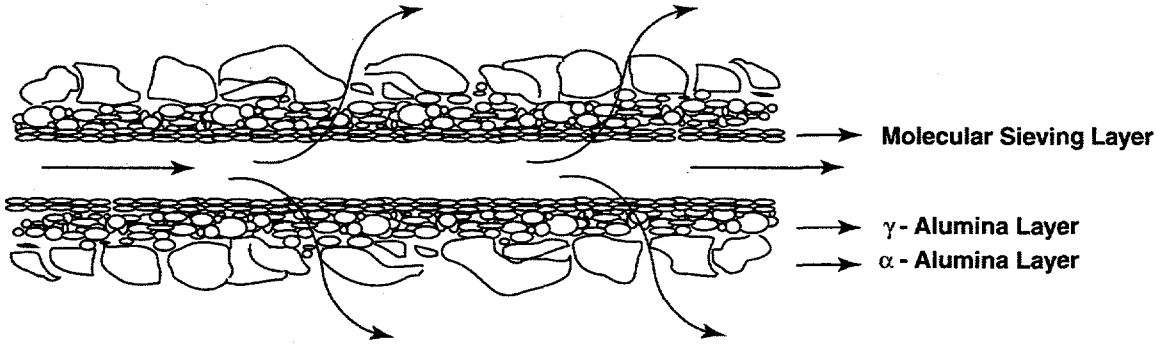

Figure 3. Schematic illustration of graded porosity tubular membrane shown in Figure 2. The molecular sieving layer can be a baseline silica membrane or a composite membrane that consists of additional layers deposited on the baseline silica membrane, which tailor the pore size and resulting permselectivity of the membrane. As illustrated in Figure 2, the annular space of the membrane tube would be filled with a packed catalyst bed for a catalytic membrane reactor application.

This project was divided into three primary tasks, briefly described as membrane development, catalyst development, and catalytic membrane reactor experiments. These tasks will be addressed as separate chapters in this report. In the first chapter, we will explore the modification of the commercial asymmetric alumina membrane tubes with microporous ceramic membrane coatings to achieve H_2 selectivity. Pure baseline (ethanol solvent-templated) silica membranes, surface-derivatized silica (composite) membranes, and surfactant-templated silica membranes (in both baseline and composite [surface derivatized] forms) were examined in this aspect of our studies. The catalytic membrane reactor concept would obviously benefit from improvements in membrane performance, either in terms of increased H_2 permeance or selectivity to H_2 relative to other potential product species. Previous experiments have shown that the modification of asymmetric alumina membrane tubes with microporous silica or titania-modified (by surface derivatization) silica composite membrane results in H_2/CH_4 separation factors of 100 to over 2000, compared to factors of 2.8 achievable with the unmodified asymmetric alumina membrane tubes [34,67]. However, considerable improvements to baseline (solvent-templated) silica microporous membrane performance, especially in terms of increased H_2 permeance, are required to meet the needs of current and future gas separation applications. Our work initially focused on reproducing these previous results, and extending the titania-modified (by surface derivatization) silica composite membrane results to baseline silica membranes modified (by surface derivatization) with ion-exchangeable HTO films. This would make it possible to impart a catalytic functionality into the membrane itself to supplement the bulk catalyst present in a membrane reactor.

A second primary task was the evaluation of bulk HTO:Si-supported dehydrogenation catalysts for use with liquid hydrocarbons typically found in gasoline. These studies were meant to identify high activity bulk catalyst materials for use in the packed catalyst bed of a catalytic membrane reactor or as thin film HTO:Si-supported catalyst materials integrated into the composite membrane structure. Rather than evaluate complex hydrocarbon mixtures, we used

model compounds, such as isooctane (2,2,4-trimethylpentane) or n-heptane, which have characteristics similar to those of gasoline. We previously investigated the use of Fe/HTO:Si and Cr/HTO:Si catalysts for dehydrogenation of isobutane and ethylbenzene, and found that the optimal catalyst formulations are similar for the two reactions [63,64]. We therefore anticipated that the use of known catalyst syntheses would yield highly active catalysts for isooctane or n-heptane dehydrogenation. Testing was performed to determine catalyst activity trends, reactant conversions, selectivities, and catalyst deactivation under various reaction conditions, and to investigate catalyst regeneration schemes. Catalyst synthesis and testing also included HTO:Si-supported noble metal catalysts as well, since supported noble metal catalysts are used in several commercially important alkane dehydrogenation/dehydrocyclization reactions (e.g., platforming, so named because it describes catalytic reforming reactions in which alkane components of petroleum-derived feeds are dehydrogenated and/or cyclized over platinum catalysts to produce more valuable [higher octane number] chemical compounds such as branched alkanes and aromatics) [68,69]. The HTO:Si-supported catalysts synthesized as part of this study were evaluated against an appropriate commercial dehydrogenation catalyst as a benchmark.

The third primary task involved joining the membrane and catalyst technologies in a single unit, and testing the performance of the resulting catalytic membrane reactor system. H_2 production rates, H_2 purity, and hydrocarbon product distributions were all measured. The ability to incorporate a catalytic function directly into the membrane offered multiple options for configuring the reactor system. The focus of our efforts in this area involved the simplest possible catalytic membrane reactor scheme, in which a microporous ceramic membrane-modified commercial asymmetric alumina membrane tube was filled with a bulk catalyst.

Chapter I. Membrane Development Efforts

Experimental

Membrane supports were prepared by sectioning commercial asymmetric 5 nm average pore diameter alumina (γ-Al_2O_3 /α-Al_2O_3) membrane tubes (U.S. Filter, Membralox®) [62] into 5.5 cm long sections, followed by ultrasonic cleaning in deionized water. These alumina membrane tubes had an OD of 1 cm and an ID of 0.7 cm. The cleaned membrane supports were then washed with deionized water several times before calcining at 450°C for 1 h.

All silica membranes of the present study were prepared from an A2** sol [67]. The A2** sol is a modification of the original A2 sol recipe developed by Brinker, et al. [70]. Preparation of the A2** sol consists of two acid-catalyzed reaction steps designed to minimize the condensation rates of silica species in order to produce weakly branched polymeric clusters that interpenetrate and collapse during film deposition to produce membranes with molecular-sized pores. The two-step procedure results in a final molar ratio of tetraethyl orthosilicate (TEOS): ethanol: H_2O: HCl =1.0: 3.8: 5.0: 0.004 (pH = 2.0, standard sol). A dip-coating sol for

solvent (ethanol)-templated silica membranes was prepared by diluting the standard sol with two times its volume of ethanol. For surfactant-templated silica membrane preparation, several surfactants were used. Some sols were prepared by adding a C6-surfactant (triethylhexylammonium bromide) powder to unaged A2** standard sol to obtain a C6-surfactant concentration of 0.125 M prior to dilution. The resulting membranes were referred to as C6-surfactant templated silica (C6STS) sublayers. Other sols were prepared by adding a C16-surfactant (cetyltrimethylammonium bromide or CTAB) powder to aged and diluted (with ethanol) A2** standard sol to obtain a final C16-surfactant concentration of 0.03-0.11 M (1.5-5 wt.%).

A sol-gel dip-coating process featuring aspects of slip casting was performed under clean conditions, including (but not restricted to) Class 100 clean room conditions. Baseline solvent (ethanol)-templated silica membranes were prepared using standard dip coating techniques (dip coating rate = 7.6 cm/min) [71]. Surface derivatization was used to further alter some of the resulting microporous silica membranes, although an HTO-like soluble intermediate (composed of NaOH/methanol/ titanium isopropoxide sol in the appropriate stoichiometry to generate a $NaTi_2O_5H$ ion exchanger) [72,73] was used in place of the pure titania coating solution (titanium isopropoxide diluted in THF) utilized in previous studies [34,67]. Prior to the surface derivatization step, the baseline silica layer was "pre-hydrolyzed" *via* soaking in deionized H_2O for 24 h. A second dip coating application was then used to apply the HTO precursor (after a 30-fold dilution in THF), and the composite membrane was heated to 400°C for 3 h in air.

Surfactant-templated silica membranes were prepared using a multi-step procedure [74]. For enhanced microstructural characterization, some samples were prepared by dip coating membranes onto single crystal silicon wafers ((100) orientation). To prepare actual surfactant-templated silica membranes for permeation testing, an asymmetric alumina membrane support tube was dip-coated using a silica sol containing the surfactant as described above. The surfactant-templated silica membranes were calcined at 120°C for 1 h in air and were confirmed to be impermeable to helium. Surfactant removal was accomplished by heating the tube at 500°C for 1 h in air. Some surfactant-templated silica membranes were further surface derivatized to produce a composite membrane material. In this case, the as-prepared asymmetric alumina membrane support tube with a surfactant-templated silica membrane sublayer was further dip-coated using an A2** sol (no added surfactant) using the standard coating procedure. The as-coated membrane tube was heated under vacuum at a rate of 1°C/min from room temperature to 300°C. Permeation measurements were conducted after performing a standard outgassing procedure (He purge at 80°C for 3 h).

Corresponding bulk xerogels were produced from the same sol precursors as the various silica membrane materials for characterization by thermal gravimetric analysis (TGA), differential thermal analysis (DTA) and nitrogen sorption porosimetry. A surface acoustic wave technique (SAW) was used to determine pore accessibility of supported films [75]. Scanning electron microscopy and transmission electron microscopy (TEM) were used to determine the morphology of membranes. Gas permeation measurements were performed in a pressure-controlled (ΔP = 80 psia) single gas or gas mixture mode without any sweep gases [67,76,77]. Flow rates were measured using a digital bubble flow meter. Gas compositions of the permeate

and retentate were analyzed by on-line gas chromatography using a thermal conductivity detector (TCD). The ideal separation factor (α_I) for various gas pairs was calculated from the ratio of individual gas permeance values obtained from measurements with either single component gases, equimolar binary gas mixtures, or a simulated reformate feed (nominal composition: 50 vol.% H_2, 1% CO, 15% CO_2, and 34% N_2).

Results and Discussion

Three major issues were initially addressed regarding the microporous silica ceramic membrane technology: integration of HTO films using a surface derivatization approach, high temperature performance of baseline silica membranes, and reproducibility of membrane fabrication.

Low temperature single gas permeance measurements were performed on these membranes both before and after HTO coating/heat treatment. The results obtained before HTO coating and heat treatment are considered representative of baseline silica membranes. These results, shown below in Figure 4, demonstrate that the permeance of all gases through the silica

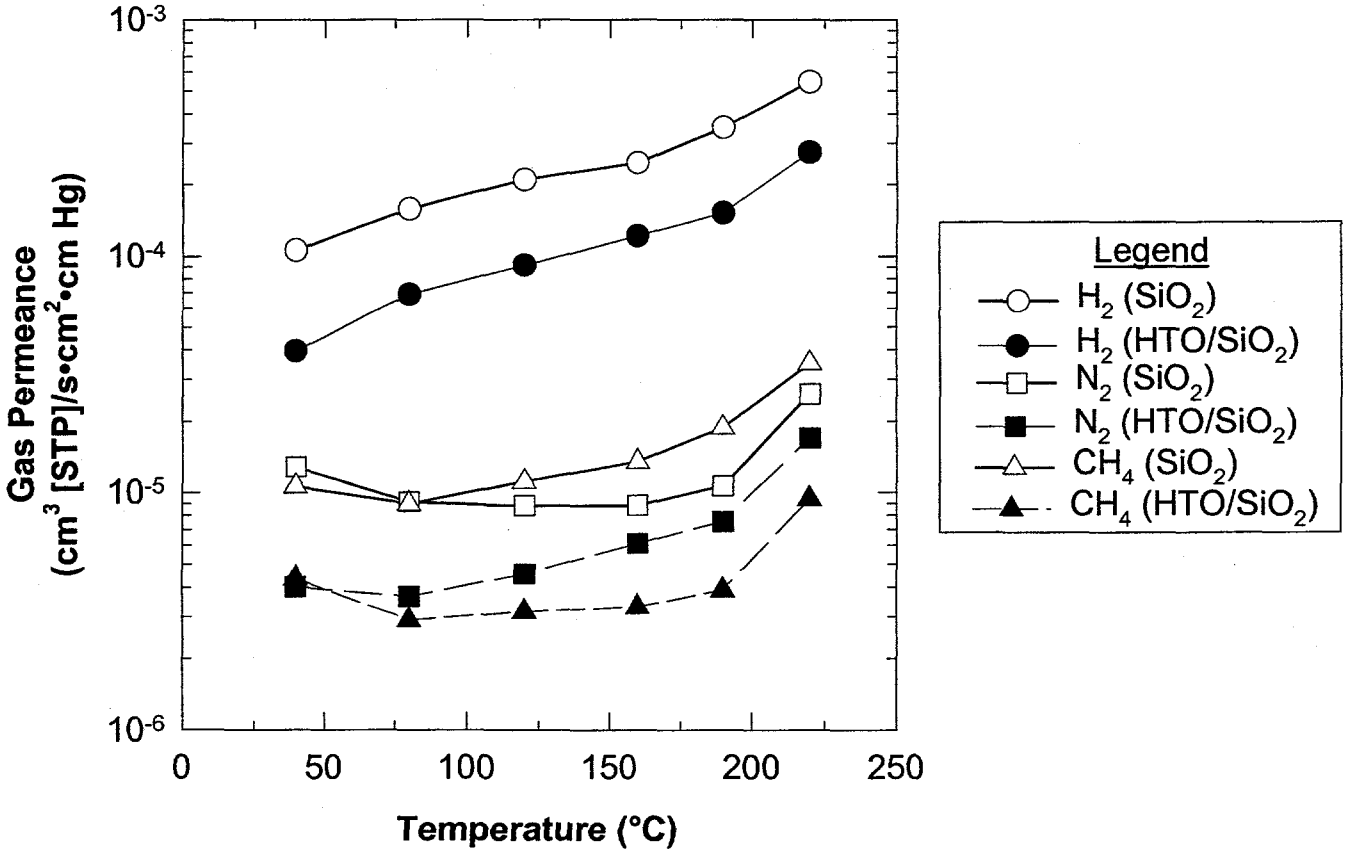

Figure 4. Low temperature single gas permeance measurement results for baseline silica microporous membranes and HTO/silica composite membranes. For simplicity, the HTO/silica composite membrane has been denoted as HTO/SiO_2 in the legend associated with the Figure.

microporous membrane was decreased by the presence of the additional HTO layer. However, concurrent with this decrease in permeance for the HTO/silica composite membrane is a slight increase in the H_2 selectivity, determined by the ratio of the single gas permeance values of H_2 versus the other gases (CH_4 and N_2). For example, the average ideal H_2/CH_4 separation factor (α_I) over the six data points shown in Figure 4 increased from ~22 for the baseline silica membrane to ~29 for the HTO/silica composite membranes. These results are consistent with more recent results (not shown herein) for surface derivatization of baseline silica microporous membranes *via* pure titania coatings.

Figure 5 below shows a typical microstructure of an HTO/silica/Al_2O_3 composite membrane prepared by this technique. In this case, the HTO layer has been designated TiO_2 and the silica layer designated as SiO_2 for simplicity.

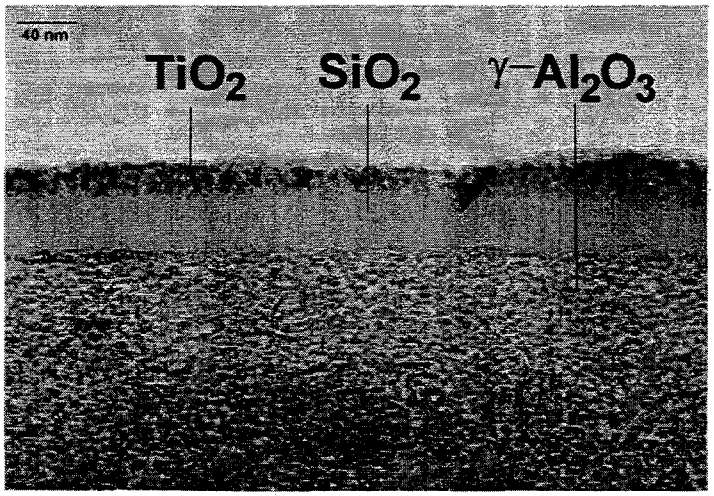

Figure 5. TEM photomicrograph showing a cross-section view of an HTO/silica composite membrane deposited on a commercial asymmetric alumina membrane tube.

In order to be used in conjunction with a dehydrogenation reaction, any membrane material (including the underlying commercial asymmetric alumina tubular membrane) must be stable to temperatures of 500-600°C that are typically used to drive the endothermic dehydrogenation reaction toward products. Nevertheless, current technology for modifying the alumina membranes had only been demonstrated at fairly low temperatures (200-300°C), and efforts were devoted to developing films that could tolerate the severe temperature environments encountered during dehydrogenation. In order to evaluate the preservation (or destruction) of the overall pore structure of the microporous silica membrane and its resulting molecular sieving capability, we performed high temperature single gas permeance measurements using baseline (solvent-templated) silica membranes as part of a study evaluating propane dehydrogenation in bulk catalyst/membrane separation systems [50]. These results, shown below in Figure 6, demonstrated a relatively large difference in gas permeance between propane (C_3H_8) and H_2 at high temperature (ideal separation factor [α_I] ~100). This data gives an excellent preliminary indication of the ability of these membranes to perform high temperature separation of H_2 from the typical products (i.e., alkenes and alkanes) resulting from alkane dehydrogenation reactions.

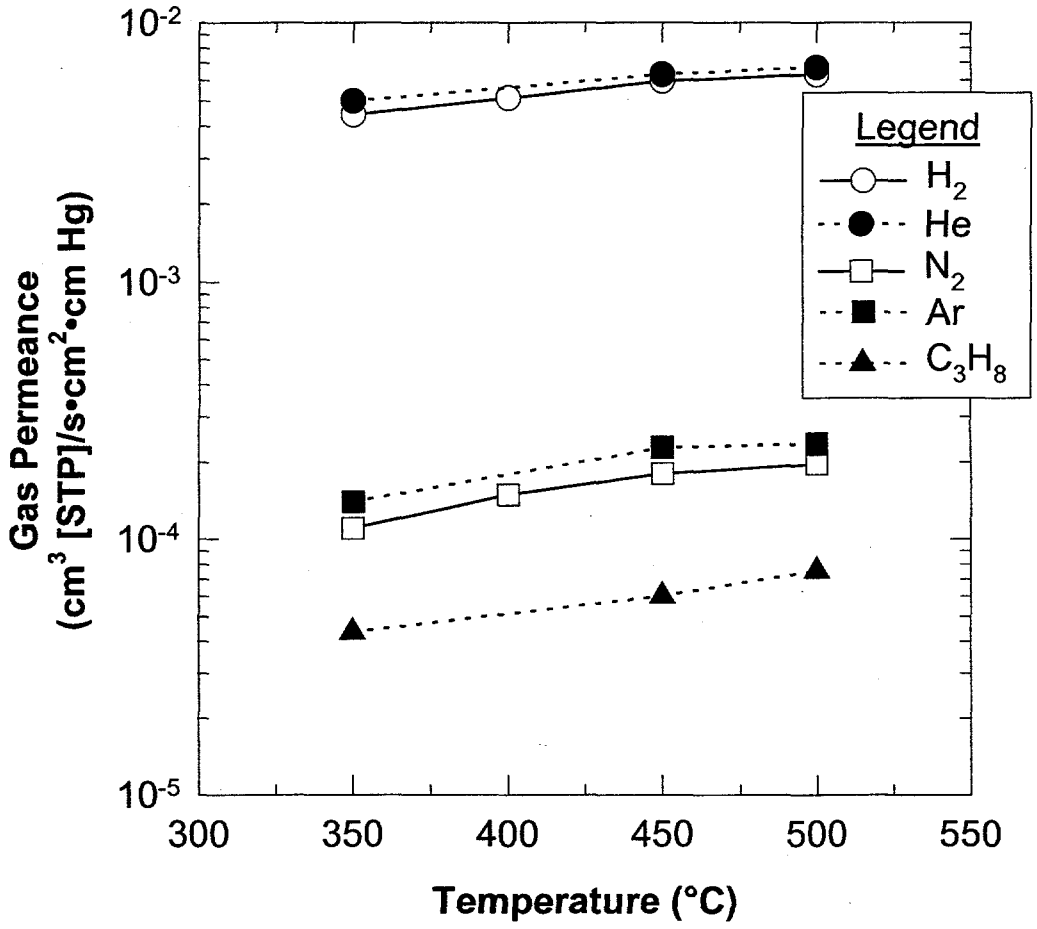

Figure 6. High temperature single gas permeance measurements for baseline silica membranes.

Regarding the reproducibility of membrane fabrication, it should be noted that the "thermal cut-off" behavior initially believed to be a characteristic of these membrane materials in baseline (solvent-templated) silica or composite titania-silica (by surface derivatization) forms [34,67] has proven to be nonreproducible. This was determined from designed experiments that were performed to isolate the effect of different silica precursor sources (TEOS suppliers) and sol ageing times on baseline (solvent-templated) silica membranes. Dip coating using these various sols was performed using two sets of conditions previously shown to produce silica membranes exhibiting "thermal cut-off" behavior [67]: (1) a very dry (< 5 ppm H_2O as evidenced by use of di-ethyl zinc and $TiCl_4$ indicators) atmosphere in the glove box used for dip coating and (2) use of a fan to assist drying of the dip-coated tubular membrane under ambient glove box conditions (air flow through the annulus of the tubular membrane). The results shown in Figure 4 for the baseline silica membranes are typical of the results observed in the further designed experiments. It is clear from the data shown in Figure 4 that no discontinuity in permeance (e.g., "thermal cut-off") is observed for any given gas molecule as a function of temperature.

This finding is significant because it was this "thermal cut-off" behavior, characterized by a complete restriction of flow for gas molecules of various size as temperature was altered, that enabled high H_2 selectivities to be obtained in the previous work [67]. The lack of reproducibility of the "thermal cut-off" behavior previously observed ultimately led us to study alternate membrane materials and fabrication techniques. Because more fundamental studies involving membrane fabrication were necessary, we abandoned further attempts to integrate an ion-exchangeable HTO film with the silica membrane materials. At some point in the future, when it has been demonstrated that microporous silica membranes with both high selectivity to H_2 and high H_2 permeance can be reproducibly fabricated, it would make sense to reevaluate the possible integration of the HTO films with these materials.

Part of these new fundamental studies involved the examination of surfactant-templated silica membrane materials, an outgrowth of work initially focused on using fugitive organic templates to increase the volume fraction of porosity in the microporous silica membrane membranes [35,36,78-80]. These new surfactant-templated silica materials showed great promise since their high porosity, ordered pore structure yielded high permeance membrane materials. Figure 7 is a TEM photomicrograph that shows the structure of a CTAB ($CH_3(CH_2)_{15}N^+(CH_3)_3Br^-$) surfactant-templated silica membrane after calcination (to remove the surfactant). This material consists of an ordered cubic liquid crystalline mesostructure, which in Figure 7 is viewed along the [100] zone axis. An orthogonal arrangement of pores is present, with a pore-to-pore distance of 7.9 nm. This illustrated that it was possible to use surfactant templating to prepare microporous and mesoporous membranes with ordered unimodal porosity (by virtue of silica/surfactant liquid crystal self-assembly during dip coating). Cubic films with

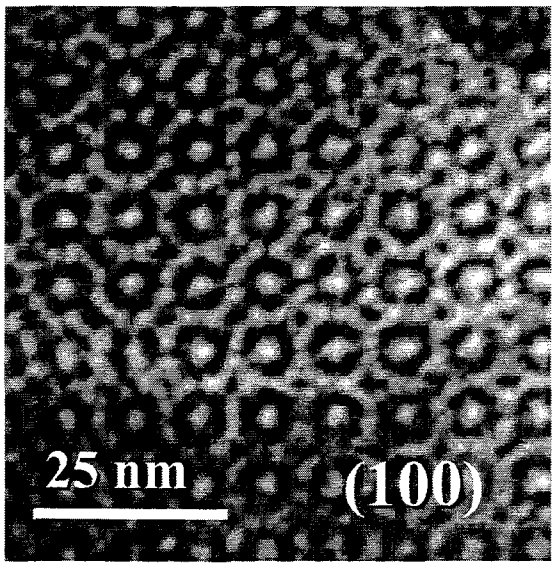

Figure 7. TEM photomicrograph of a surfactant-templated silica film as viewed along the [100] zone axis. This photomicrograph demonstrates that the material consists of an ordered cubic liquid crystalline mesostructure.

3-dimensional pore channel systems are excellent candidates for inorganic membranes because, similar to zeolites, the pore size is monodisperse, the pore tortuosity (transmembrane transport path length/film thickness) equals one, and the pore volume fraction can be varied in the range of 30-60% (compared to 10-20% for baseline [solvent-templated] silica membranes). The as-deposited membranes (before surfactant removal) were leak tight and after calcination (500°C/1h/air) the flux increased by over 3 orders of magnitude [74].

To be used for H_2 separation, the pore size (diameter) of the surfactant-templated silica membranes needed to be reduced from > 1 nm to a target of < 0.4 nm by utilization of a surface derivatization step, reducing surfactant molecule size, or perhaps collapsing micellar pores in a controlled fashion. We investigated the use of a surface derivatization step using well-defined metal alkoxide clusters to reduce the pore size of the topmost layer of the surfactant-templated silica membrane. We hoped to limit the derivatized region to a very thin layer in order to achieve composite membranes that retain the low pore tortuosity and unimodal pore size of the parent surfactant-templated silica sublayer.

Surface derivatization of the C16 surfactant templated silica membrane was performed using the A2** sol. This procedure produced composite membranes with increased low temperature (< 200°C) H_2 permeance values relative to baseline solvent (ethanol)-templated A2** sol-derived membranes and H_2/CH_4 permselectivity values ranging from 90 to 200. Although these were promising results, the large pore size (average pore diameter ~1.8 nm) resulting from the initial C16 surfactant template limited the ability of the surface derivatization technique to refine the pore size enough to enable the production of composite membranes with high H_2 selectivities. For this reason, smaller surfactant molecules, like triethylhexylammonium bromide, were used in an effort to generate ordered arrays of smaller pores. In principle, these pores would still be large enough to allow high permeances to be obtained, but would be small enough that surface derivatization techniques would be more effective in producing high H_2 selectivities. The surfactant-templated silica membranes prepared using this C6 surfactant produced an initial pore size (diameter) in the calcined film of 1.0-1.2 nm compared to the ~1.8 nm pores observed in the case of the C16 surfactant-templated silica films.

Although amenable to permeation or microscopic evaluation, thin film membrane coatings are very difficult to characterize by conventional means (e.g., thermal analysis, surface area, etc.) due to the limited quantity of material present. In order to perform more effective materials characterization, bulk xerogel samples were prepared using the same chemistry as that employed to synthesize membrane coatings. For the as-prepared C6STS xerogel, differential thermal analysis (DTA) showed that an endothermic peak near 200°C corresponded to the beginning of a drastic weight loss indicating the decomposition of the C6-surfactant template. An exothermic peak at around 350°C, accompanied by a weight loss of about 45%, signified the oxidative pyrolysis of surfactant and residual organics (see Figure 8). N_2 sorption isotherms of the calcined C6STS thin film (calcined at 500°C for 1 h in air), determined using a surface acoustic wave (SAW) technique, appeared to be Type I, characteristic of microporous materials (data not shown).

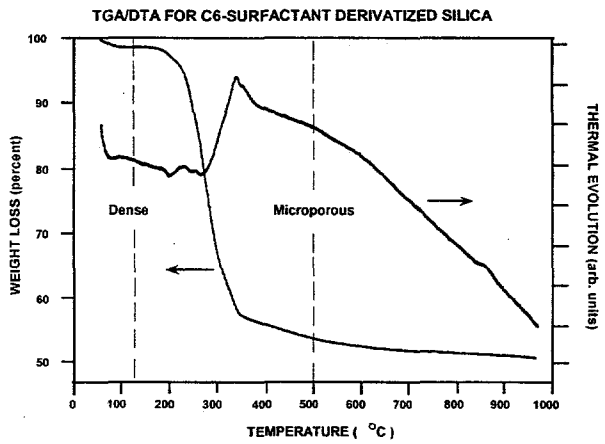

Figure 8. Weight loss and heat evolution of C6STS xerogel during thermal gravimetric analysis (TGA) and differential thermal analysis (DTA) in air (1 atm) at a heating rate of 2°C/min. The dashed lines indicate the calcination temperatures used to prepare materials for nitrogen adsorption and gas permeation measurements.

This new processing procedure (C6 surfactant templating + surface derivatization using an A2** sol) resulted in both high flux and selectivity for the membranes with gradual changes of pore size (diameter) from 5.0 nm (commercial γ–alumina support layer) to 1.0-1.2 nm (surfactant-templated silica sublayer), and then to 0.3-0.4 nm (ultramicroporous silica top-layer) [81]. Electron micrographs which illustrate the cross-section and the surface of the supported composite silica membrane are shown in Figure 9. The thickness of the defect-free ultramicroporous A2** layer was around 30 nm.

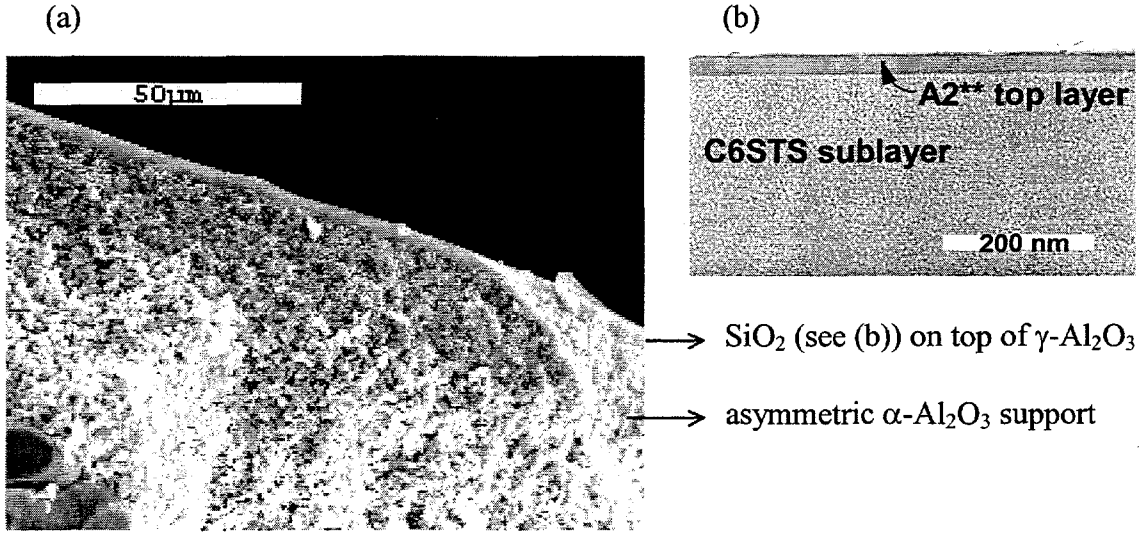

Figure 9. Cross-sectional electron micrographs of a silica membrane prepared by C6 surfactant templating + surface derivatization: (a) SEM overview of the membrane, (b) TEM micrograph reveals the detail of the separate silica layers.

The C6STS sublayer may serve to (1) eliminate intrinsic defects on commercial porous supports and promote pore uniformity; therefore, increasing selectivity, or (2) prevent penetration of a subsequently deposited ultramicroporous membrane (e.g. A2** sol-derived membrane with a pore size [diameter] of 0.3-0.4 nm), thus enhancing flux. We compared gas permeances and selectivities for A2** membranes with or without a C6STS sublayer. After standard vacuum calcination at 300°C, the membrane with a sublayer exhibited four-fold higher CO_2 permeances and four-fold higher CO_2/CH_4 selectivities than that without a sublayer at 60°C in a pure gas permeation measurement. The vacuum calcination procedure apparently resulted in the decomposition of surface ethoxy groups; therefore, an inner pore surface with better hydrophobicity might have been formed as evidenced by an increase in water contact angle on the membrane surface (data not shown herein). The membrane was capable of discriminating gas molecules such as He (kinetic diameter 0.26 nm), H_2 (0.289 nm), CO_2 (0.33 nm), CH_4 (0.38 nm), and N_2 (0.364 nm) *via* a molecular sieving mechanism. Ideal separation factors (ratio of single gas permeance values) for various gas pairs (e.g., α_I (CO_2/CH_4) = 102) significantly exceeded Knudsen separation factors (e.g., α_K (CO_2/CH_4) = 0.6). Moreover, due to selective adsorption of CO_2, a remarkably high CO_2 permeance (3.2 x 10^{-4} cm^3(STP)/[s·cm^2·cm Hg]) and a CO_2/CH_4 separation factor of 200 was achieved at 26°C for an equimolar CO_2/CH_4 gas mixture. The combination of high permeance and high selectivity exceeded that of the best known gas separation membranes (e.g., asymmetric polyimide with a typical CO_2/CH_4 separation factor of 55 and a CO_2 permeance of 1.7 x 10^{-4} cm^3(STP)/[s·cm^2·cm Hg]) on the market [82].

The above membrane was further calcined at 450°C for 1 h in air. Single gas permeation results at 80°C are shown in Figure 10. Due to the extended calcination, the pore size of the membrane was further reduced, resulting in a sharp molecular size cut-off at ~0.35 nm. With an excellent hydrogen separation factor (H_2/CH_4 = 1265) as well as a high hydrogen permeance (1×10^{-3} cm^3(STP)/[cm^2·s·cm Hg]), such a membrane provides a great opportunity in applications such as hydrogen recovery from petrochemical plants and hydrogen purification for fuel cells. The membrane selectively separated H_2 from a simulated reformate gas feed (33.98% N_2, 15.00% CO_2, 0.997% CO, balance H_2) for fuel cells as evidenced by the high concentration of hydrogen recovered in the permeate side stream (see Table 1). A 92 mole% H_2 purity could be obtained in the permeate stream at a stage-cut of 8.2% (stage-cut is defined as the ratio of the permeate to feed volumetric flow rates). The CO concentration (CO is a known PEM fuel cell poison) in the permeate was reduced at least a factor of fifty times relative to the simulated reformate feed. The observed selectivities in this experiment with a simulated reformate feed are more realistic than the calculated ideal selectivity values from the single gas permeance measurements shown in Figure 10.

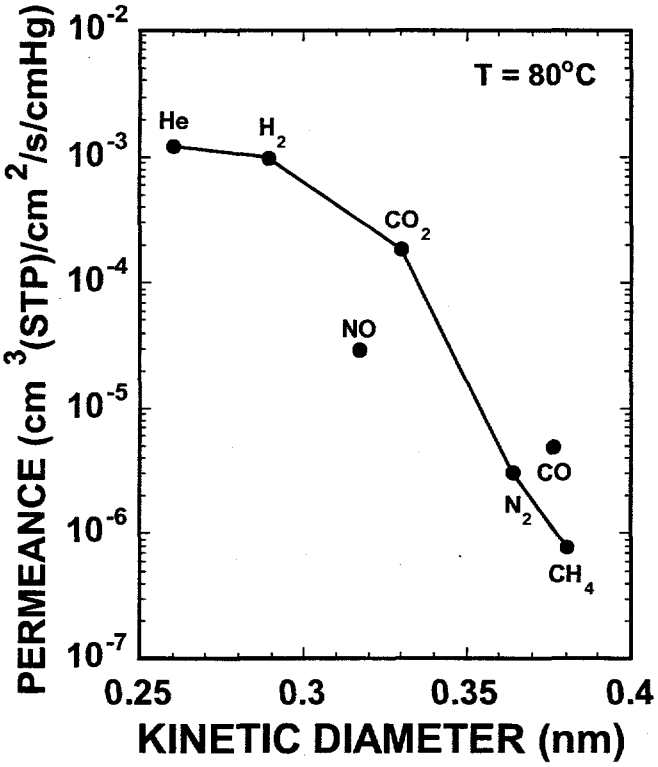

Gas Pair	*Ideal Separation Factor, α_I*
He/CH_4	1530
H_2/CH_4	1265
CO_2/N_2	60
CO_2/CH_4	240
NO/N_2	9.3

Figure 10. Molecular sieving behavior of an A2** sol-derivatized C6STS membrane calcined at 450°C for 1 h in air. The ideal separation factor, α_I, represents the ratio of permeance values (measured in single gas permeance tests) for the two specified gases.

Table 1. Permeances of components of a simulated reformate product gas mixture* at 80°C.

Gas i	Permeance × 10^6 (cm^3 (STP)/s·cm^2·cm Hg)	Separation Factor (H_2/Gas i)	Pure gas permeance ratio	Permeate (mole%)	Retentate (mole%)
H_2	507	-	-	92.19	43.25
CO_2	101	5.0	5.2	7.36	16.89
N_2	2.15	235.9	316.0	0.37	40.47
CO	3.83	132.2	198.6	0.0193	1.14

Notes:

* Simulated reformate feed gas mixture composition: 50.023% H_2, 15% CO_2, 33.98%N_2, 0.997% CO.

A tube-side pressure of 80 psig was used for all measurements.

Summary

This study determined that it was possible to integrate ion-exchangeable HTO films into the structure of composite microporous ceramic membranes and that the baseline (solvent-templated) silica membranes still exhibited molecular sieving behavior at high temperatures (> 400°C). Unfortunately, it was also determined that the "thermal cut-off" behavior previously observed for both baseline silica and surface derivatized silica (titania/silica) was non-reproducible. This finding resulted in a return to more fundamental studies related to microporous ceramic membrane fabrication.

The quality of the support is crucial to the quality of overlying membrane layer. Pinholes and surface roughness on the support normally produce defects in the subsequently deposited layer. We designed a new protocol to improve membrane performance and reproducibility. First, we deposited a surfactant-templated microporous or mesoporous intermediate layer on top of a commercial asymmetric alumina membrane support to both improve surface finish and prevent the subsequently deposited silica sol used for surface derivatization from penetrating into the support. Second, membranes were dip-coated under Class 100 clean room conditions to avoid dust contamination and were calcined to promote further pore shrinkage. This new procedure resulted in both high flux and selectivity for the membranes with gradual changes of pore size (diameter) from 5.0 nm (commercial γ–alumina support layer) to 1.0-2.0 nm (surfactant-templated silica sublayer), and then to 0.3-0.4 nm (30 nm thick, ultramicroporous silica top-layer). The subject membranes are capable of molecular sieving and could find great use in applications such as purification of subquality natural gas, reduction of green house gases (e.g. CO_2) and hydrogen recovery from processing gases and feedstocks.

Chapter II. Bulk Catalyst Development Efforts

Experimental

Silica-doped sodium titanate supports were prepared using previously described sol-gel methods. [65,66,72,73,83]. In all cases, the Na:Ti ratio was adjusted to a value of 1:2 to maximize ion exchange capacity and tetraethyl orthosilicate (TEOS) was added to give a Si:Ti ratio of 1:5. The presence of silica greatly stabilizes support surface area during subsequent high temperature processing. The empirical formula for this as-prepared silica-doped sodium titanate ion exchanger is $NaTi_2O_5H$:0.4 SiO_2, while the acronym HTO:Si is generically used to describe the final catalyst support.

HTO:Si-supported Cr catalysts [63] were prepared by first equilibrating the $NaTi_2O_5H$:0.4SiO_2 material at a desired pH ranging from 5.2-7.5 using HCl, then adding a solution of the metal salt (0.12 M $Cr(NO_3)_3$) containing a two to three-fold excess of metal (beyond the theoretical ion exchange capacity of the $NaTi_2O_5H$:0.4 SiO_2 support) with mild

stirring. After one hour, the resulting Cr/HTO:Si was filtered, washed with water and acetone, and dried under house vacuum (3-5 in. Hg) at room temperature. Separate acidification procedures were not necessary to remove residual non-exchanged Na^+ from the catalyst precursors due to the combination of the large excess of Cr^{+3} used in the ion exchange procedure, the long equilibration time allowed for cation exchange, and the relatively low pH used for ion exchange.

To prepare HTO:Si-supported Pt-based catalysts, a single large batch of a nominal 1 wt.% Pt/HTO:Si catalyst material (calcined basis) was prepared and subsequently doped with Sn and Re to prepare Pt-Sn/HTO:Si and Pt-Re/HTO:Si catalyst materials. The initial 1 wt.% Pt/HTO:Si catalyst material was prepared using standard techniques [84]. Briefly, 0.96 g of $Pt(NH_3)_4(NO_3)_2$ was dissolved in 750 ml of deionized water, and 80 g of $NaTi_2O_5H$:0.4 SiO_2 powder was added to form a slurry. Following slurry formation, the pH was lowered to 5.5 using 10 wt.% HNO_3 and held there for 10 min by adding 10 wt.% HNO_3 dropwise as needed. The slurry was then filtered using a coarse porosity glass frit Buchner funnel and rinsed with DI water. Because this Pt loading represents only a small portion of the overall cation exchange capacity of the $NaTi_2O_5H$:0.4 SiO_2 material, the initial ion exchange product material contained a relatively large quantity of residual sodium (> 2 wt.%). Therefore, separate acidification was required to remove this residual sodium to produce a low sodium (< 0.5 wt.% Na^+ on a calcined basis) Pt/HTO:Si catalyst material. For acidification, the filter cake from the original ion exchange procedure was redispersed in 750 ml DI water to form a slurry and then additions of 10 wt.% HNO_3 were used to lower the pH of the slurry to 3.9, where it was held for a period of 3 min. Following this treatment, the slurry was filtered and rinsed with deionized water as described above. The acidification procedure was repeated a total of three additional times. After the final acidification and water rinse, the filter cake was rinsed three times with acetone and vacuum dried at room temperature.

Catalyst precursor materials were analyzed for metal content by atomic absorption spectrophotometry (AAS), volatiles contents were determined by weight loss measurements in conjunction with standard calcination treatments, and surface areas were measured by N_2 adsorption using the BET method (both before and after standard calcination treatments). The as-prepared catalyst precursor powders were granulated to a size range of -60/+80 mesh. This was accomplished by first pressing a 1.125 in. dia pellet (~2 g) using a pressure of 12 kpsi. Light grinding with a mortar and pestle was then used to generate the desired mesh fraction. The Pt-based/HTO:Si catalyst granules were calcined at 600°C for 2 h (heating rate = 5°C/min up to 550°C, then 1 °C/min from 550 to 600°C) in stagnant air.

Pt-Re/HTO:Si and Pt-Sn/HTO:Si catalysts (both containing 1:1 weight ratios of Pt:Re or Sn) were prepared by doping the calcined Pt/HTO:Si granules with appropriate Re and Sn precursors, respectively. In the case of the Pt-Re/HTO:Si catalyst, 0.07 g of NH_4ReO_4 was dissolved in 4.4 ml deionized water, with the resulting solution carefully added to 5.0 g of calcined Pt/HTO:Si granules. After overnight drying at room temperature in air, followed by drying at 100°C in air for 2 h, the Pt-Re/HTO:Si catalyst precursors were calcined at 600°C for 2 h in stagnant air as previously described. In the case of the Pt-Sn/HTO:Si catalyst, 5.0 g of calcined Pt/HTO:Si granules were impregnated using 4.4 ml of a solution of a 0.095 M Tin (IV)

2,6-bis-isopropylphenoxide ($Sn[2,6\text{-}OC_6H_3(CH(CH_3)_2)_2]_4$) in toluene. Subsequent drying and calcination treatments were identical to those previously described for the Pt-Re/HTO:Si catalyst.

In the case of the Pt-based/HTO:Si catalysts, all granulated samples loaded into the reactor for testing were previously calcined at 600°C. In contrast, the Cr/HTO:Si catalyst granules were loaded into the reactor in the as-prepared form (without any heat treatment above room temperature) and heat treated *in situ* prior to catalyst testing. Consequently, significant catalyst weight loss and shrinkage of the catalyst bed volume in the flow reactor were observed for the Cr/HTO:Si catalysts relative to the Pt-based/HTO:Si catalysts, which exhibited no significant shrinkage. In all cases, space velocity values are referenced to the final catalyst bed volumes or weights as appropriate.

Activity measurements were made in a conventional atmospheric pressure packed bed flow reactor shown schematically in Figure 11 [63,85]. Gases were fed through calibrated mass flow controllers and up to two gases could be fed at any time (only one mass flow controller is shown in the figure for clarity). The system was capable of handling both gas and liquid feeds, with an HPLC pump used to control liquid feed rate. Only liquid feeds, either pure isooctane or pure n-heptane, were used in this study. The reactants entered a high temperature oven, and were preheated and mixed (if multiple feeds were used) in a 1/8 in. dia coiled stainless steel tube at the reactor inlet. The preheated reactants then entered a 3/8 in. dia stainless steel tube (wall thickness 0.065 in.) containing the packed catalyst bed. The catalyst was supported on a fine steel mesh located at the bottom of the reactor. Depending on catalyst density, volatiles content, and estimated shrinkage, 2-4 g of granulated (-60/+80 mesh) catalyst were typically used to give a nominal final catalyst bed volume of 3.6 cc. Actual final catalyst bed volumes ranged from 3.1-4.1 cc. Reactant flow rates were adjusted to provide weight hourly space velocity (WHSV) values of 0.6-3.0 g feed/(g catalyst·h), using the final weight of the catalyst sample (after testing) as a reference. This helped normalize differences in volatiles content among the various samples. The corresponding range of liquid hourly space velocity (LHSV) values was 0.8-3.8 cc feed/cc catalyst·h). Reaction temperature ranges utilized for this study were 590-600°C for isooctane dehydrogenation experiments, and 525-575°C for n-heptane dehydrogenation/dehydrocyclization. After exiting the reactor, product gases were exhausted through the sample loop of a gas chromatograph, where C1-C4 hydrocarbons were analyzed relative to known standards using a flame ionization detector (FID). Since this gas chromatograph was not equipped with a TCD, no direct measurements of H_2 production could be made. Liquid samples were condensed by cooling with an ice bath, and the collected liquids were analyzed by gas chromatography using an FID and mass spectrometry relative to known standards. Reactor temperature was measured by three thermocouples externally attached to the top, middle, and bottom of the reactor, and one thermocouple located inside the reactor at the bottom of the catalyst bed. No significant differences were ever observed among the four thermocouples indicating that the reactor operated in an isothermal mode. In addition to the Cr/HTO:Si and Pt-based/HTO:Si catalysts, a commercial 7.5 wt% $Cr/\gamma\text{-}Al_2O_3$ catalyst (Girdler G-41, supplied by United Catalysts, Inc.) was also tested as a benchmark.

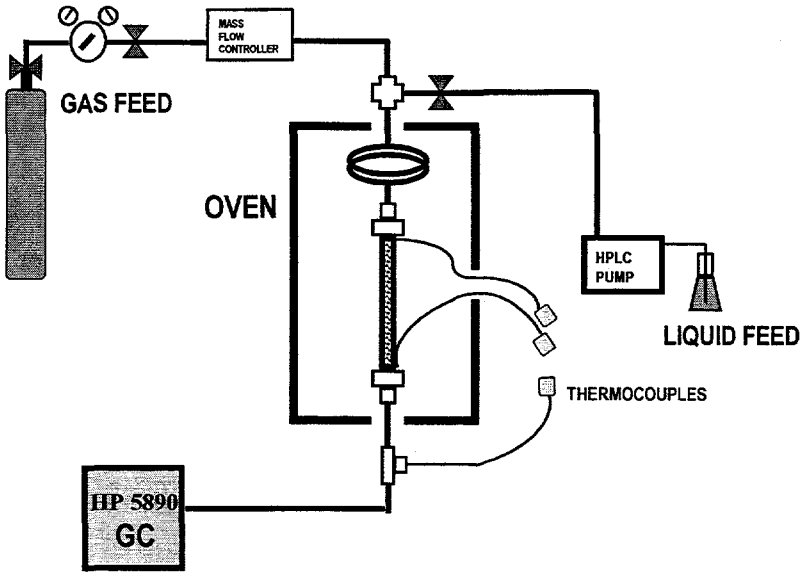

Figure 11. Schematic diagram of conventional packed bed dehydrogenation reactor.

A typical reaction sequence began with heating of the catalyst bed to reaction temperature in flowing nitrogen. Once temperature was reached, the nitrogen flow was stopped and reactant flow begun. Product stream sampling and analysis for both gas and condensed liquid species was typically performed at 20 min intervals. For the Pt-based/HTO:Si catalysts, reduction treatments in pure hydrogen (at 500-550°C for 0.5-1 h) were used to activate the catalysts *in situ* prior to dehydrogenation testing. For all catalysts, air oxidation at 550°C for times ranging from 10 min to 2 h was used to regenerate the catalysts at periodic intervals. After completion of a reaction sequence, the reactant flow was shut off and the reactor was cooled to room temperature in flowing nitrogen. After conclusion of a reactor test, the catalyst was removed from the reactor and saved for surface area analysis.

Results and Discussion

Preliminary Isooctane Dehydrogenation Screening Experiment

For this initial screening experiment, a 1.6 wt.% Fe/HTO:Si catalyst (EBL87, Fe loading reported on an as-prepared basis) previously used for ethylbenzene dehydrogenation (to styrene) [63,64] was evaluated for hydrogen generation *via* isooctane dehydrogenation to olefin products. The most likely liquid isooctane (2,2,4-trimethylpentane) dehydrogenation products are 2,4,4-trimethyl-1-pentene and 2,4,4-trimethyl-2-pentene, with reaction to each of these products generating one mole of H_2. At a reaction temperature of 600°C and a WHSV of 0.5-1.5 h^{-1}, less than 2% of the total isooctane fed to the reactor as liquid was converted to liquid dehydrogenated

products. However, significant conversion of isooctane to gaseous products was observed, indicating the presence of cracking reactions. These cracking reactions were undesirable since they produced non-selective products (C1-C5 alkanes and alkenes) which not only significantly reduced the hydrogen yield, but ultimately required separation from the desired H_2 product. The presence of extensive branching in isooctane and the absence of multiple C-C single bonds that can be dehydrogenated not only resulted in a low ratio of dehydrogenation to cracking, but also limited the total amount of hydrogen that could be produced (even if cracking was eliminated).

Our results were a bit surprising since it has been reported that trimethylpentanes reacted over chromia/alumina [86,87] form xylenes *via* skeletal rearrangement (isomerization) and aromatization reactions. The active phase (iron oxide) and the HTO:Si support are significantly different from a chromia/alumina catalyst and could possibly explain our observed results. Rather than further pursue the isooctane dehydrogenation strategy, we chose to focus our attention on the use of n-heptane dehydrogenation/dehydrocyclization as a model reaction.

Heptane Dehydrogenation/Dehydrocyclization Experiments

The dehydrogenation/dehydrocyclization of n-heptane is a more suitable choice as a model reaction for catalyst testing for two reasons: 1) it yields a significant quantity of hydrogen; and 2) it has been well studied. The conversion of normal alkanes to aromatic compounds represents an important class of catalytic reforming reactions, which are primarily used to produce high research octane number (RON) branched or aromatic compounds to improve the antiknock properties of gasoline blends. This is dramatically illustrated by comparing the RON values for the C7 hydrocarbons n-heptane (0) and toluene (124) [68,69,86].

The net chemical reaction for dehydrogenation/dehydrocyclization of n-heptane to toluene is illustrated below in Figure 12.

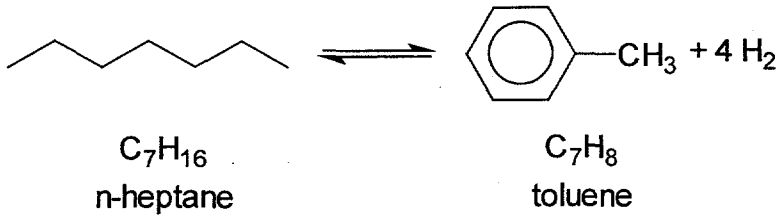

Figure 12. Net chemical reaction for dehydrogenation/dehydrocyclization of n-heptane to toluene.

Several different types of reactions can occur in a dehydrocyclization scheme (e.g., the formation of toluene from n-heptane); different catalytic sites can be involved, including metallic active sites (e.g., Pt or Cr_2O_3) and acidic sites on the support. Under typical reforming conditions (high operating pressures including a significant partial pressure of H_2), possible reaction paths can include a metallic monofunctional path, a metallic bifunctional path, and an acid bifunctional

path, depending on the specific catalyst/support characteristics and reaction conditions [69,88]. The metallic monofunctional path involves a single metallic active site and a cyclohexanic intermediate which can be rapidly dehydrogenated to form toluene, although several groups still postulate a mechanism involving paraffin dehydrogenation to diolefin or triolefin species before cyclization [89]. For example, over chromia/alumina catalysts, Steiner [87] has shown that dehydrogenation reactions are suppressed by H_2, resulting in direct n-heptane cyclization to form a naphthene (six carbon member ring) intermediate (e.g., methylcyclohexane), consistent with this metallic monofunctional route. The metallic bifunctional pathway involves both metallic and acid active sites, with cyclization of a 5 carbon ring intermediate (e.g., ethylcyclopentane or dimethylcyclopentanes) on the metallic site followed by gas phase migration to and ring expansion on the acid site (carbonium ion mechanism), and a final dehydrogenation step on the metallic site. The acid bifunctional pathway is supposed to take place on acid sites *via* olefins or diolefins produced from paraffin. Acid sites become increasingly important at higher reaction temperatures (> 425°C) [90]. For all of these routes, cyclization is believed to be the probable rate determining step. In contrast, for the use of neat n-heptane feeds run over chromia/alumina catalysts at or near atmospheric pressure (nontypical reforming conditions), it has been shown that an initial slow catalytic dehydrogenation step to produce an olefin (e.g., 1-heptene) occurs, followed by a rapid cyclization step to produce toluene [86,87].

Catalysts based on alumina-supported metal oxides of the titanium, vanadium, and tungsten groups of the periodic table [86,87], as well as supported Pt-based catalysts [69,89-92], are well known to promote the dehydrogenation/dehydrocyclization reactions of normal alkanes [86,87]. A significant complicating factor affecting catalyst performance (activity, selectivity, and deactivation) is the fact that different types of metallic, metal oxide, and acid active sites have the ability to catalyze a wide range of possible competing reactions, including hydrogenolysis or cracking (cleavage), isomerization (cationic skeletal rearrangements), and hydrogenation. Aromatics are the most stable hydrocarbon species at temperatures above 250°C, and above 400°C equilibrium is displaced far enough toward aromatic products that even considerable pressures of H_2 do not significantly suppress dehydrogenation reactions [87]. Typical reaction conditions involve temperatures in the 450-550°C range and a wide range of pressures [68]. No equilibrium limitations exist (at atmospheric pressure) for the n-heptane dehydrogenation/dehydrocyclization reaction to toluene at 550°C. Part of the rationale for using this particular reaction temperature (550°C) was to compare the n-heptane dehydrogenation/dehydrocyclization results to previous propane dehydrogenation test data obtained at 550°C, for which equilibrium limitations exist.

Supported Cr Catalysts

The active phase in supported Cr catalysts is generally acknowledged to be chromium oxide (Cr_2O_3), which is also referred to as chromia. Although descriptors such as Cr/Al_2O_3, chromia/alumina, or Cr/HTO:Si will be used interchangeably in this report to denote the respective catalyst formulations, these different terms do not imply that distinct supported Cr active phases exist in each case. As stated above, it is expected that Cr_2O_3 is the active phase in all of the supported Cr catalysts studied herein.

Commercial Benchmark Catalyst - Girdler G-41 Cr/Al_2O_3

This material was a 7.5 wt.% Cr/γ-Al_2O_3 catalyst material (Girdler G-41, supplied by United Catalysts, Inc.) and was considered an effective benchmark representative of commercial dehydrogenation catalysts. This Cr loading is equivalent to ~11 wt.% Cr_2O_3. The primary application of this catalyst is for hydrodealkylation of toluene to benzene or substituted naphthalenes to naphthalene [93].

Heptane dehydrogenation/dehydrocyclization testing of this catalyst immediately followed propane dehydrogenation testing performed in conjunction with a separate project [85]. Experience with other supported Cr catalysts has shown that initial propane dehydrogenation testing does not significantly alter catalyst test results in subsequent heptane dehydrogenation/dehydrocyclization tests. For this catalyst, propane conversions to propylene at 550°C were found to be equilibrium limited (25-30% conversion), with a selectivity of 83-90%, illustrating the effectiveness of this dehydrogenation catalyst. Theoretical calculations based on thermodynamic data indicate an equilibrium conversion of 30% at a temperature of 540°C for propane dehydrogenation to propylene [86,94].

Following propane dehydrogenation testing, the reactor was purged with N_2 for 100 min at 550°C, while the HPLC pump was flushed and primed with the heptane liquid feed. After initial heptane dehydrogenation/dehydrocyclization testing as a function of time-on-stream, the heptane flow was terminated, a N_2 purge was performed, and an air regeneration step at 550°C for 1 h was performed. Heptane dehydrogenation/dehydrocyclization testing was then continued after a subsequent N_2 purge. Several sequential regeneration cycles were performed, followed by heptane dehydrogenation/dehydrocyclization testing at alternate temperatures (525 or 575°C) or weight hourly space velocities (WHSV, ranging from 2.0-3.0 g heptane/g catalyst·h). Unfortunately, no blank experiments without catalyst loaded in the tube or with the various catalyst support materials were performed to determine whether thermal reactions, reactions occurring on the reactor tube walls, or reactions occurring on the support (i.e., acid sites) were important relative to the contribution of the active phase. However, based on previous propane [85] and isobutane [63] dehydrogenation experiments, the effect of the catalyst was expected to dominate all other possible contributions.

Table 2 summarizes the n-heptane dehydrogenation/dehydrocyclization results obtained with the Girdler G-41 catalyst. This catalyst shows reasonable activity for heptane conversion to toluene that is stable with a number of air regeneration cycles. One of the key parameters shown in Table 2 is the toluene selectivity, which indicates the mole % of the original n-heptane feed converted to toluene. This is the most desired liquid product since n-heptane conversion to toluene as described by Figure 12 yields significant amounts of H_2. However, the data shown in Table 1 show that significant nonselective side reactions are occurring since only 35-50% of the total n-heptane fed to the reactor is converted to toluene. This could possibly be attributed to significant contributions of acid sites on the high purity γ-Al_2O_3 support toward cationic skeletal rearrangements and cleavage reactions. This is consistent with the large amount of gaseous

products observed at all reaction conditions for this catalyst and also the high concentration of C1-C4 alkanes (relative to alkenes) present in this gas product. These high alkane/alkene ratios (3 to 4.5) in the gaseous products might also result from the fact that some hydrogen generated by the dehydrocyclization reaction is consumed to rehydrogenate product alkenes or to "cap" cracking products. Comparison of the toluene and total combustible liquid yield data in Table 2 indicates that most of the product liquid analyzed after condensation is composed of toluene.

Table 2. Heptane dehydrogenation/dehydrocyclization results obtained with the Girdler G-41 7.5 wt.% $Cr/\gamma\text{-}Al_2O_3$ catalyst.

Stage of Testing[+]	Reaction Temp. (°C)	WHSV (h^{-1})	Total Heptane Conversion (%)[@]	Total Combustible Liquid Yield (%)[#]	Total Toluene Yield (%)[$]	Total Toluene Selectivity (%)[^]	Alkane in Gas Product (%)[&]
Initial*	550	2.04	67.1	31.6	26.5	39.4	78.8
Regen. #1	550	2.04	62.1	36.4	30.5	49.1	NA
Regen. #2	550	2.04	59.6	33.0	27.2	45.5	80.8
Regen. #3	525	2.04	47.2	27.2	19.2	40.7	NA
Regen. #4	575	2.04	76.1	27.0	22.9	30.1	NA
Regen. #5	550	2.96	44.0	27.6	19.2	43.8	NA

Notes:

[+] All tabulated values represent data corresponding to a time-on-stream of 40 min for the specified conditions, except for the higher WHSV condition (2.96 h^{-1}), where the data correspond to a time-on-stream of 30 min.

[@] Total heptane conversion is based on the disappearance of heptane into both liquid and gas products.

[#] Total combustible liquid yield is based on the moles of heptane reacted to produce liquid products.

[$] Total toluene yield is based on the moles of heptane reacted to produce toluene.

[^] Total toluene selectivity represents the moles of toluene produced relative to the total moles of heptane converted to both liquid and gas products.

[&] % alkanes in the gas product was determined by the concentration of C1-C4 alkanes present in the gas product relative to all gaseous species produced.

* Initial heptane dehydrogenation/dehydrocyclization testing followed propane dehydrogenation testing at 550°C and air regeneration. No significant catalyst deactivation was observed due to propane dehydrogenation testing.

Toluene comprised 75-85% of the liquids collected with the remainder (listed in order of decreasing concentration) consisting of small quantities of benzene (dealkylation product), various heptenes (dehydrogenation intermediates), dimethylcyclopentanes (C5 cyclization pathway products), and pentanes (cracking or dealkylation products). The presence of benzene is

not a surprise since the primary application of the Girdler G-41 catalyst is for hydrodealkylation of toluene to produce benzene [93].

Steiner has extensively reviewed the literature with respect to aromatization reactions over supported Cr catalysts [87]. Typical laboratory conditions for aromatization of neat n-heptane feeds at near atmospheric pressure involve temperatures ranging from 450-550°C. At 475°C, gas contact times of a few sec to ~1 min yielded conversions of n-heptane to toluene of 95%, with < 5% of the feed converted to cracking products. Only unconverted n-heptane, 1-heptene, and toluene were observed in the condensed liquid effluent from the reactor [87,95]. Higher temperatures are reported to lead to nonselective cracking reactions. Pines has also pointed out the importance of using alkali metal additions to alumina supports to poison acid sites, decreasing the selectivity toward cracking reactions [86]. Our study utilized a high purity (non-alkali metal containing) γ-Al_2O_3-supported Cr catalyst with short gas contact times (5-10 sec) at relatively high temperatures (525-575°C). The combination of the significant acid sites on the Girdler G-41 alumina support and the high temperatures utilized probably led to significant nonselective cracking reactions and decreased performance relative to previous literature studies.

The reaction temperature had significant effects on catalyst performance. Calculation of the apparent activation energy from the total heptane conversion data at 525-575°C yielded a value of ~13 kcal/mole. Although total heptane conversion increased significantly over this temperature range, the production of toluene was optimized at 550°C, which validated the selection of this reaction temperature as the standard condition. Increasing the WHSV by increasing the heptane flow rate to the reactor had a predictable effect on total heptane conversion, even though the observed conversions were high with respect to typical differential operation conditions (< 10% conversion). Under differential operation conditions in a plug flow reactor, conversion should be inversely proportional to the reactant flow rate. Appropriate calculations comparing the total heptane conversion observed for the final stage of testing at a WHSV of 2.96 h^{-1} and 550°C (44.0%) show excellent agreement with that predicted using the differential reactor operation assumption in conjunction with the overall average total heptane conversion for the first three stages of testing (see Table 2) at a WHSV of 2.04 h^{-1} and 550°C (43.8%).

Table 2 does not show data relative to catalyst deactivation as a function of time-on-stream at a given reaction temperature. Deactivation data for this catalyst will be presented in the next section on Cr/HTO:Si catalysts so that the performance of the two types of catalyst materials can be compared. With this overall test data as a baseline, a series of Cr/HTO:Si catalysts were synthesized and evaluated with the goal of obtaining higher conversions and hydrogen generation rates than the commercial Girdler G-41 7.5 wt.% Cr/γ-Al_2O_3 catalyst.

Cr/HTO:Si Catalysts

Figure 13 shows the chromium loading versus pH for the four Cr/HTO:Si samples studied. The Cr loading was found to increase in a quasi-linear fashion with loading pH. Cr

loading varies by nearly a factor of two over the range of pH studied. This increase in Cr loading with increasing pH is likely explained by either more effective Cr^{+3} exchange for Na^+ (relative to H^+ exchange for Na^+) at higher pH or perhaps by the formation of cationic hydrolyzed Cr species of various charge at the higher pH conditions [96], which also can participate in cation exchange reactions. However, localized polymerization/precipitation of Cr species at the surface of the HTO:Si material is also possible at higher pH. All of the as-prepared Cr/HTO:Si catalysts had very low levels (< 0.1 wt.%) of residual Na^+, indicating nearly complete Na^+ removal from the original $NaTi_2O_5H$:0.4 SiO_2 ion exchange material.

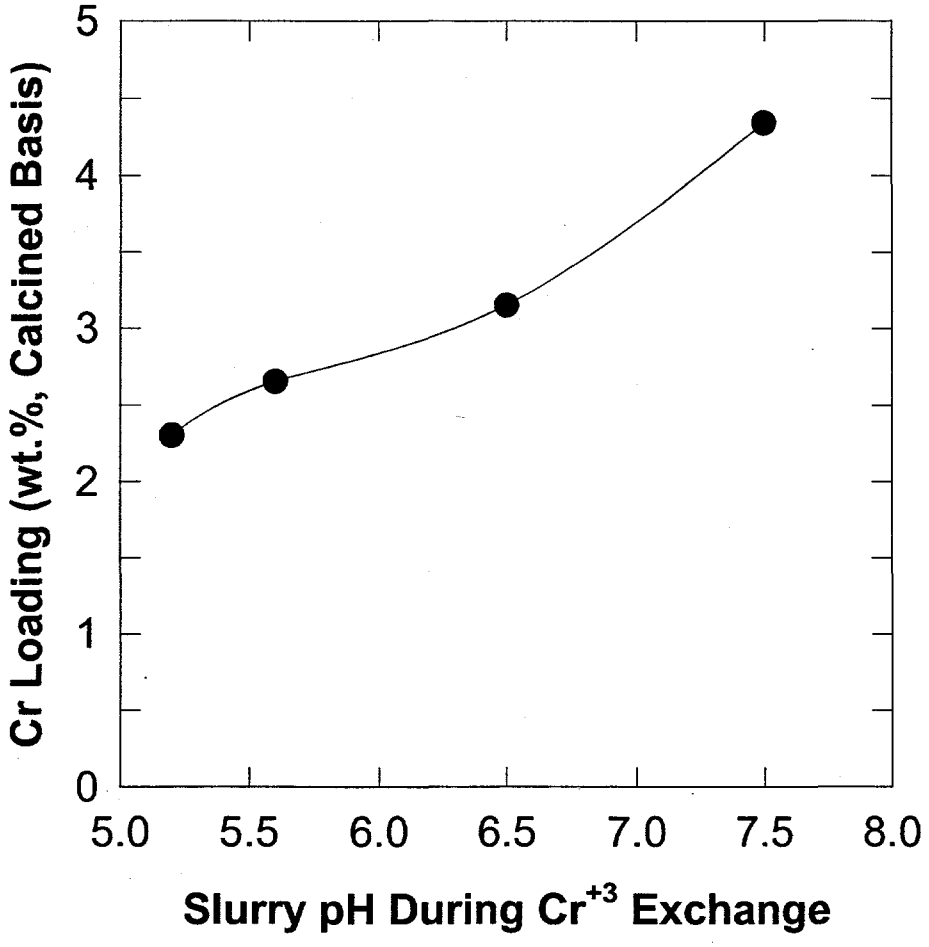

Figure 13. Variation of chromium loading on HTO:Si supports with pH used during the cation exchange procedure.

Figure 14 shows the heptane dehydrogenation/dehydrocyclization activity (in terms of both total and specific [per g Cr] heptane conversion) of the Cr/HTO:Si catalysts at 550°C normalized to a constant weight hourly space velocity (WHSV) of 2.0 h^{-1}. These values represent the initial activity data for the catalysts (time-on-stream = 30 min). Note that no blank run (no catalyst) was performed for the n-heptane dehydrogenation/dehydrocyclization reaction; therefore, no data is reported for 0% Cr loading as in previous work [63,85]. The data show that

increased Cr loading had only a slight effect on total heptane conversion over the range of loadings studied, with optimum activity observed for Cr loadings in the 2-2.5 wt.% (calcined basis) range. However, it can be noted that these conversion values are significantly lower than that obtained for the Girdler G-41 7.5 wt.% Cr/γ-Al_2O_3 catalyst, which is included in Figure 14 for comparison.

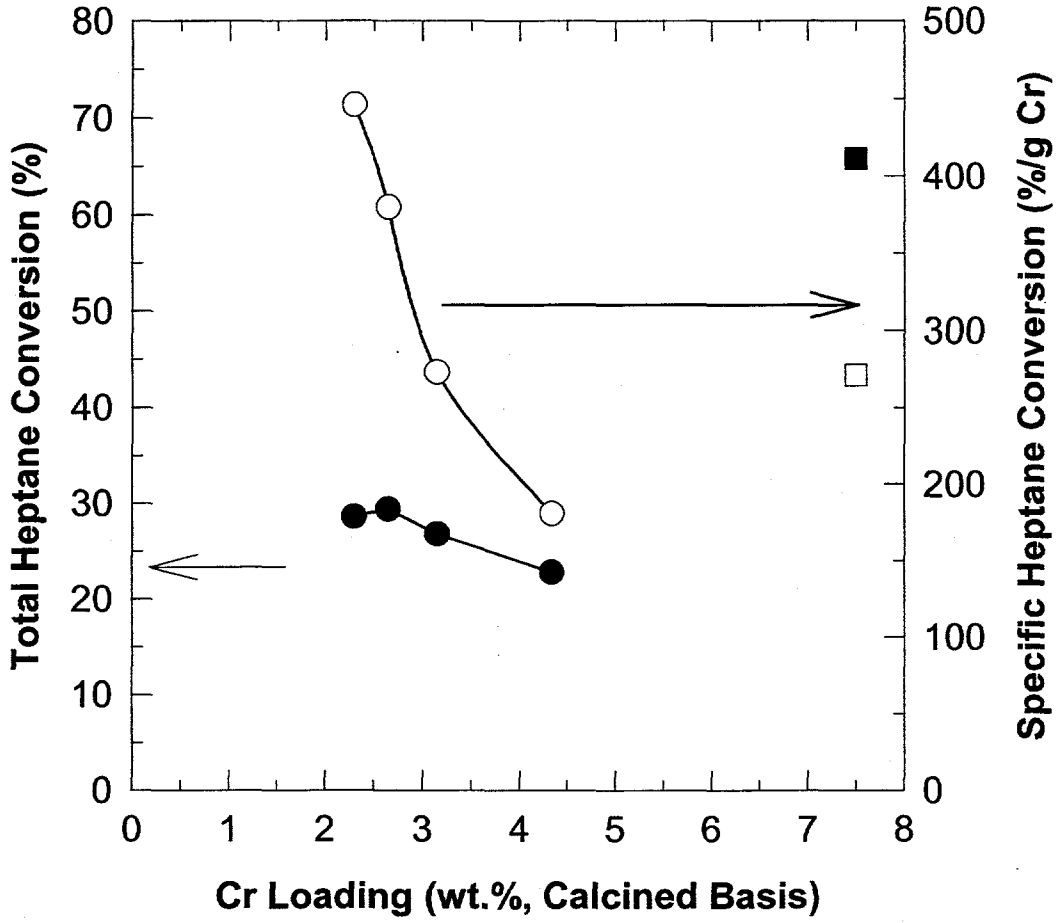

Figure 14. Initial total and specific (per g Cr) heptane dehydrogenation/dehydrocyclization activity of Cr/HTO:Si and Girdler G-41 7.5 wt.% Cr/γ-Al_2O_3 catalysts at 550°C, WHSV = 2.0 h^{-1}. Filled symbols correspond to total heptane conversion data while open symbols correspond to specific heptane conversion data. Circular symbols correspond to Cr/HTO:Si catalyst data while square symbols correspond to the Girdler G-41 catalyst data.

Examination of the specific heptane conversion data shown in Figure 14 reveals a steady decrease in activity with increasing Cr content for the Cr/HTO:Si catalysts. It should be noted that this decrease in specific activity also corresponds to an increase in the slurry pH used for the Cr^{+3} ion exchange step. This behavior could therefore be the result of differences in the chemical state of the Cr loaded at different pH values, or due to the formation of larger, less well-dispersed Cr_2O_3 particles at higher pH, which would offset the effects of higher Cr loading. However, the steady decrease in specific activity with increasing Cr loading is very consistent with the decrease

in dispersion of the active Cr phase expected with increased Cr loading. Transmission electron microscopy (TEM) or some other independent evaluation of Cr dispersion (e.g. magnetic susceptibility [87]) would be required to verify this speculation. Nevertheless, the fact that overall heptane conversion activity significantly decreases with increasing Cr loading makes it unlikely that further improvements could be achieved in the Cr/HTO:Si catalysts. Similar trends in specific catalyst activity have previously been observed for Cr/HTO:Si catalysts used in both propane and isobutane dehydrogenation experiments, although overall catalyst activity was insensitive to Cr loading in these two previous cases [63,85].

Although not shown in Figure 14, it is worth noting that toluene selectivities were not significantly affected by increased Cr loading for the Cr/HTO:Si catalysts. Increased Cr loading on the HTO:Si ion exchangers was effected by increasing the pH at which the HTO:Si was equilibrated prior to Cr exchange. Therefore, increases in Cr loading could possibly have been accompanied by a decreased acidity of the catalyst and therefore a decrease in the fraction of the feed stream converted to gaseous products by cracking reactions. However, it is possible that the effect of the decreased Cr dispersions observed with increasing Cr loading (as evidenced by the significant decreases in specific activity with increasing Cr content shown in Figure 14) dominated any possible changes in support acidity for the Cr/HTO:Si catalysts with higher Cr loadings.

These results are not consistent with the case of Fe/HTO:Si catalysts for ethylbenzene dehydrogenation [63,64], where a very sharp maximum in bulk activity with increasing iron loading was observed at a loading of ~1.6 wt.% (as-prepared basis). This maximum was attributed to the formation of a particular ion-exchanged iron species within a very narrow pH window. The slightly higher total heptane conversion observed in the 2-2.5 wt.% Cr loading range is far less dramatic than that observed in the case of the Fe/HTO:Si catalysts used for ethylbenzene dehydrogenation [63,64].

It is obvious from the heptane conversion data described above that the Cr/HTO:Si catalysts compared poorly with the commercial Girdler G-41 7.5 wt.% Cr/γ-Al_2O_3 catalyst. Corresponding total toluene selectivities also compared unfavorably with the Girdler G-41 catalyst; values of only 10-20% were achieved at these reaction conditions for all Cr/HTO:Si catalysts. These overall toluene selectivities corresponded to ~50% selectivity to toluene in the liquid products, significantly lower than that observed for the Girdler G-41 catalyst (~75%). Consistent with this fact, a large number of small peaks were observed *via* gas chromatography of the liquid products; however, time was not taken to identify all of these individual species since the activity of the Cr/HTO:Si catalysts was low relative to the Girdler G-41 catalyst. The Cr/HTO:Si materials yielded gaseous alkane/alkene ratios of only 2 to 3, lower than those observed for the commercial Girdler G-41 catalyst (see Table 2). This indicated that these Cr/HTO:Si catalysts may rehydrogenate a smaller fraction of the alkene products. Overall, the low toluene and combustible liquid yields observed for the Cr/HTO:Si catalysts indicate a strong presence of cationic skeletal rearrangement and cleavage (cracking) reactions, therefore decreasing the selectivity of the catalyst toward aromatization. This might be due to the presence of acid sites in the HTO:Si support resulting from Ti-O-Si bonding [66]. Since lower Cr loadings were used for these catalysts this might lead to a lower fraction of the HTO:Si support

surface being covered with the active Cr phase, therefore allow greater acid site participation in the non-selective (to aromatization) conversion of n-heptane.

Several possible explanations exist to explain the difference in activity and selectivity for the Cr/HTO:Si catalysts relative to the commercial 7.5 wt.% $Cr/\gamma\text{-}Al_2O_3$ (Girdler G-41) catalyst. In terms of catalyst activity on an overall or specific (per g Cr) basis, Figure 14 shows that the Girdler G-41 catalyst is significantly more active than the Cr/HTO:Si catalysts. This could be due to the significant difference in chemistry between the high purity $\gamma\text{-}Al_2O_3$ and HTO:Si supports used for these catalysts. Following Na^+ removal and heat treatment, the amorphous HTO:Si support crystallizes to form TiO_2 phases (anatase, brookite, or rutile), although the addition of the SiO_2 dopant helps preserve high surface area by retarding the crystallization of the low temperature, high surface area TiO_2 polymorphs (anatase and brookite) to the low surface area, high temperature stable rutile phase. Characterization of the surface area of the various catalysts (by N_2 adsorption using the BET method) revealed that after a 600°C calcination treatment in air for 2 h, the surface areas of the Cr/HTO:Si catalysts ranged from 140-165 m^2/g, compared to a value of 185 m^2/g for the Girdler G-41 catalyst. If the x-axis of Figure 14 were replotted to show Cr loading per m^2 of catalyst surface area, the plot would look the same. Thus, one cannot explain the superior activity of the Girdler G-41 catalyst solely on a support surface area basis. Another possible explanation might be related to a superior ability of the high purity $\gamma\text{-}Al_2O_3$ relative to TiO_2 to disperse Cr/Cr_2O_3 phases. Also, the acidity of these different supports may play an important role in both the activity and selectivity of these different catalysts. A detailed discussion of the possible differences in support acidity between the high purity $\gamma\text{-}Al_2O_3$ and HTO:Si supports has been given elsewhere [66]. Significant further work would be required to identify the fundamental differences between these two catalysts responsible for the observed differences in catalyst activity and selectivity.

The commercial 7.5 wt.% $Cr/\gamma\text{-}Al_2O_3$ catalyst and the Cr/HTO:Si catalysts were also compared in the area of catalyst deactivation with increasing time-on-stream. It is well established that commercial catalysts deactivate under typical industrial reaction conditions, requiring periodic air regeneration treatments to restore catalyst activity. It would be an obvious benefit to develop more deactivation-resistant catalysts for industrial chemical production. $Cr/\gamma\text{-}Al_2O_3$ catalyst deactivation data reported by Steiner showed that the concentration of toluene in the product decreases by a factor of 4x over a time-on-stream period of 2 h. It was also reported that the rate of catalyst deactivation could be significantly reduced by including a substantial partial pressure of H_2 in the feed. Under industrial reformer conditions, high-pressure operation (including a significant partial pressure of H_2) with recycle of a portion of the product is typically utilized.

Figure 15 shows total heptane conversion data as a function of time-on-stream at a reaction temperature of 550°C and a nominal WHSV of 2 h^{-1}. The performance of the 2.65 wt.% Cr/HTO:Si catalyst was selected as representative of all of the Cr/HTO:Si catalysts. The initial catalyst deactivation and catalyst performance after one air regeneration treatment at 550°C in air are shown in Figure 15. Further cycling of the catalyst under similar conditions revealed very similar results. The large activity difference between the Girdler G-41 and the 2.65 wt.% Cr/HTO:Si catalysts previously shown in Figure 14 are also illustrated in this figure. The Girdler

G-41 catalyst showed significant deactivation on initial exposure to the n-heptane feed, appearing to be slightly more stable after the first and subsequent (data not shown) air regeneration treatments. Although the Cr/HTO:Si catalyst appears to be more stable against catalyst deactivation, the Girdler G-41 catalyst in its most deactivated state is still more active than the Cr/HTO:Si catalyst. One other interesting feature observed for the Cr/HTO:Si catalyst was a factor of two increase in toluene yield with increasing time-on-stream over a 1 h period. This might be consistent with the poisoning of acid sites on the HTO:Si support, resulting in decreased activity for cationic skeletal rearrangement and cleavage reactions, therefore improving selectivity toward toluene.

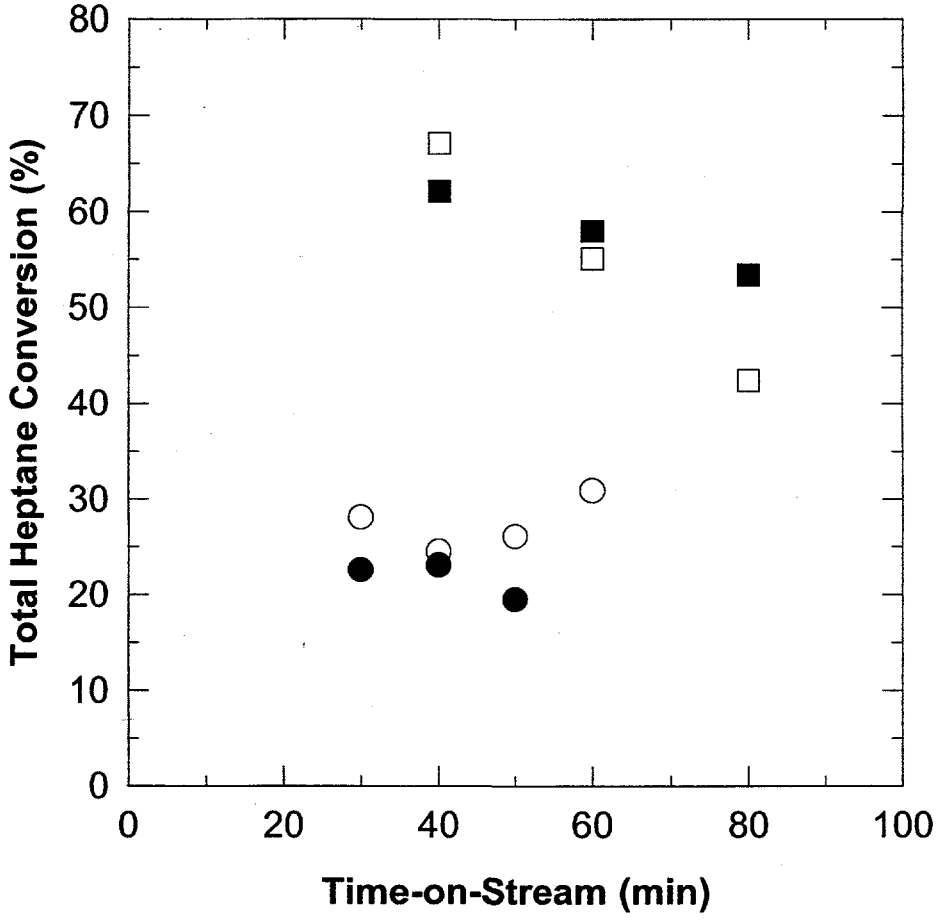

Figure 15. Total heptane conversion as a function of time-on-stream at 550°C and a nominal WHSV of 2 h^{-1} for the Girdler G-41 7.5 wt.% Cr/γ-Al_2O_3 (square symbols) and the 2.65 wt.% Cr/HTO:Si (circular symbols) catalysts before and after air regeneration. Open symbols represent initial catalyst deactivation and filled symbols represent catalyst deactivation after one air regeneration treatment at 550°C.

Two final aspects of catalyst deactivation to be considered are the weight and surface area changes for the various supported Cr catalysts tested. All of the as-prepared Cr/HTO:Si samples had very large surface areas (350-450 m^2/g), as described previously [63,73]. These materials

undergo significant surface area reduction (to 140-165 m^2/g) and volatiles removal (22-28 wt.%) during a standard calcination procedure (600°C/2h/air). Calcination of the Girdler catalyst under similar conditions showed ~10 wt.% loss (probably due to adsorbed moisture) and a negligible change in surface area. By combining the volatiles content and surface area data for the Cr/HTO:Si catalysts, it was possible to estimate the weight and surface area after reaction for these materials, assuming no changes due to coking/catalyst deactivation. For all of the Cr/HTO:Si catalysts, the observed weight loss ranged from 17-21 wt.%, significantly lower than the expected volatiles contents for these materials. This indicated that the Cr/HTO:Si catalysts experienced a net wet gain due to coking on the order of ~3-9%. Concurrent with this coking was a significant reduction in surface area; surface areas of the Cr/HTO:Si samples removed from the reactor ranged from 100-120 m^2/g, ~25% below the values for the calcined samples. This decrease is also consistent with coking of the catalyst, which easily fills the smaller pores responsible for the high surface area of these materials. A low temperature (100-150°C) was used to outgas these samples prior to surface area measurements to ensure that the carbonaceous deposits were not significantly volatilized. For comparison, the Girdler G-41 catalyst also was observed to lose less weight than expected after exposure to reaction conditions, indicating a net wet gain due to coking on the order of ~5%. The percentage of surface area reduction for this material relative to its calcined only form was nearly identical to that of the Cr/HTO:Si materials.

Thus, the most important finding from this section is that the commercial Girdler G-41 7.5 wt.% Cr/γ-Al_2O_3 catalyst is clearly more active than the Cr/HTO:Si catalysts. The inability to increase the activity of the Cr/HTO:Si catalysts through increased metal loading leads to the conclusion that Cr/HTO:Si catalysts are unlikely to provide any benefit over currently available technology.

Pt-Based/HTO:Si Catalysts

A wealth of literature exists with respect to Pt-based reforming catalysts [68,69,86,89-92]. Industrial catalysts have acidic functionality designed into the catalyst support. It is believed that dehydrogenation/hydrogenation reactions are largely structure-insensitive (no significant particle size, shape, or surface structure/irregularities effect on activity or selectivity) and can proceed even on the smallest ensembles of active sites, possibly even single Pt atoms [86,90]. If aromatization is viewed as consecutive dehydrogenation, similar behavior might be expected. Consistent with this argument is the fact that these reactions are least affected by carbonaceous deposits, sulfur poisoning, or alloying of Pt with inactive components [90].

However, the overall scheme of possible competing reactions within a catalytic reformer, including hydrogenolysis, isomerization, hydrogenation/dehydrogenation, C5 cyclization, and aromatization, is complicated not only by the large variety of possible reactions but also by the fact that some of these reactions are structure-sensitive (particle size, shape, or surface structure/irregularities significantly affects activity or selectivity, e.g., hydrogenolysis), while others are structure-insensitive (e.g., dehydrogenation) [97-99]. Also, activity for these varied reactions is highly dependent on the specific reforming conditions (temperature, pressure, H_2 concentration, presence of poisons, etc.) as well as other characteristics of the catalyst (choice of

metal and support acidity). These complications make it extremely difficult to draw general conclusions regarding optimum catalyst characteristics with respect to the overall dehydrocyclization/dehydrogenation scheme. Several authors have observed a possible increase in catalyst deactivation due to carbon deposition (also referred to as self poisoning) with large Pt particles, but interpretation of these results has been difficult due to many of the complications described above [90].

The initial n-heptane dehydrogenation/dehydrocyclization data for the Pt-based catalysts after a H_2 reduction treatment at 500-550°C for 0.5-1 h is shown in Table 3. In one case, denoted as Pt/HTO:Si*, heptane dehydrogenation/dehydrocyclization activity evaluation at 550°C followed propane dehydrogenation activity testing at 550°C. This was done to clearly tie the current Pt/HTO:Si catalyst development efforts with earlier propane dehydrogenation studies involving inverse micelle/sol-gel formulated Pt/SiO_2 and Pt/Al_2O_3 catalysts [85]. All Pt catalysts used herein had a nominal Pt loading of 1.0 wt.% (calcined basis), with the Pt-Re/HTO:Si and Pt-Sn/HTO:Si catalysts having a 1:1 weight ratio of Pt:Re (atomic ratio ~1:1 Re:Pt) or Pt:Sn (atomic ratio ~1.6:1 Sn:Pt). The reactor conditions were chosen so as to compare the heptane dehydrogenation/dehydrocyclization activity and selectivity data of the Pt-based/HTO:Si catalysts with that observed for the Cr/HTO:Si and 7.5 wt.% Cr/γ-Al_2O_3 catalysts also evaluated as part of this study.

Initial evaluation of the 1.0 wt.% Pt/HTO:Si catalyst for propane dehydrogenation at 550°C showed that 20-30% conversion of propane and high selectivity to propylene (90-100%) were obtained. Equilibrium limited conversion was observed for this catalyst at nominal WHSV values of 2-4 h^{-1} (corresponding gas hourly space velocity [GHSV] values were nominally 3-6 cc feed/(cc catalyst·h)), consistent with the results obtained for the 7.5 wt.% Cr/γ-Al_2O_3 (Girdler G-41) catalyst. This propane dehydrogenation result represents a significant improvement over the inverse micelle/sol-gel formulated Pt/SiO_2 and Pt/Al_2O_3 catalysts investigated in a previous study, although these latter catalysts contained lower Pt contents (nominal loading 0.3 wt.% on a calcined basis) and were tested at relatively high WSHV values ($\geq 4\ h^{-1}$) [85].

The first observation that can be made regarding the data in Table 3 is that the total heptane conversions obtained for the Pt-based/HTO:Si catalysts are significantly lower than those obtained for the Girdler G-41 catalyst (see Table 2) and slightly lower than those obtained for the Cr/HTO:Si catalysts (see Figure 14) run under nearly identical conditions. As expected, on a specific activity basis (per atom Cr or Pt), the Pt-based/HTO:Si catalysts are more active than the Girdler G-41 catalyst. However, bulk catalyst activity on an overall weight or volume basis is the critical factor used to screen catalysts for industrial applications. Alkane concentrations in the gas product ranged from 60-70%, similar to the values observed for the Cr/HTO:Si catalysts. Overall, it may not be fair to compare the performance of Pt and Cr catalysts at the same operating conditions since considerable previous work has shown that different operating conditions (temperature, etc.) are required for optimum results with each type of catalyst [86].

The major difference in reforming conditions required for Pt-based catalysts relative to Cr- or Mo-based catalysts is the use of high operating pressures (10-30 atm total, including a

significant H_2 partial pressure) and lower temperatures. Supported Pt catalysts show an increased selectivity to formation of C5 ring products (i.e., ethylcyclopentane and dimethylcyclopentanes) compared to the six member carbon ring products (e.g., benzene and toluene) at lower temperatures (< 300°C) and at increased H_2 pressure at a given reaction temperature [86,89]. Hydrogenolysis and isomerization selectivity were both high for Pt catalysts in heptane reactions with H_2 at 275°C, relative to cyclization reactions [90,92]. On the other hand, aromatization rates (six member carbon ring product formation) have been shown to increase with increasing temperature (regardless of H_2 pressure) [89]. This implies that in the case of aromatization, moderate H_2 pressures promote the formation of six member carbon ring products by removing carbonaceous deposits *via* hydrogenation. However, in the case of C5 cyclization, the sharp decrease in product formation at low H_2 pressures implies that H_2 must be an active participant in the surface intermediate involved in C5 cyclization [89].

Table 3. Heptane dehydrogenation/dehydrocyclization results obtained with the Pt-based/HTO:Si catalysts.

Catalyst[+]	WHSV (h^{-1})	Time on Stream (min)	Total Heptane Conversion (%)[@]	Total Combustible Liquid Yield (%)[#]	Total Toluene Yield (%)[$]	Total Toluene Selectivity (%)[^]	Alkane in Gas Product (%)[&]
Pt/HTO:Si*	2.40	50	21.8	10.9	4.5	20.9	60
Pt/HTO:Si	2.69	50	17.5	11.2	4.2	24.1	63
Pt-Re/HTO:Si	2.42	50	26.6	13.7	5.8	21.9	72
Pt-Sn/HTO:Si	2.43	50	20.2	15.3	7.8	38.5	65

Notes:

[+] All tabulated values represent the initial data corresponding to a reaction temperature of 550°C for the specified conditions. A time-on-stream value of 50 min was chosen for comparison based on the availability of all activity and selectivity data. WHSV values were not normalized for data comparison purposes.

[@], [#], [$], [^], [&] The definitions for these symbols are similar to those defined in Table 1.

* Initial heptane dehydrogenation/dehydrocyclization evaluation followed propane dehydrogenation testing at 550°C. Prior to propane dehydrogenation testing at 550°C, this catalyst was heat treated at 500°C/H_2/1h. Following propane dehydrogenation testing and prior to n-heptane dehydrogenation/dehydrocyclization evaluation, this catalyst was cooled to room temperature in N_2, reheated to 550°C in N_2, and heat treated in H_2 for 1 h at 550°C. No significant catalyst deactivation was observed due to the propane dehydrogenation testing or the multiple reduction treatments.

The role of hydrogen pressure in reforming reactions, including n-heptane dehydrocyclization, over supported Pt catalysts has been reviewed in detail by Bournonville and Franck [69]. Hydrogen pressure has an important, but complex, effect on reforming activity.

When the H_2 pressure decreases at constant hydrocarbon pressure, the rate of dehydrocyclization increases up to a maximum and then tends toward zero for low H_2 pressures. This provides evidence that a competition exists between H_2 and hydrocarbons for the active sites on the metal particles, which is further explained by the following two points: (1) at low pressures, H_2 acts by limiting the concentration of highly dehydrogenated species on the catalyst surface, which are known coke precursors; and (2) at high pressures, through adsorption, H_2 reduces the number of vacant sites that are available for cyclization as well as the concentration of dehydrogenated intermediates necessary for cyclization. It is important to point out that this effect is independent of catalyst ageing.

The reactor conditions used herein are more representative of optimum conditions used for n-heptane dehydrogenation/dehydrocyclization over supported Cr catalyst materials. In general, lower temperatures (< 400°C) are more optimum for supported Pt catalysts [86]. Equally unfortunate was the fact that no commercial Pt catalyst benchmark was run under identical conditions to compare with the activity of the Pt-based/HTO:Si catalysts. Because of the high temperature used for n-heptane dehydrogenation/dehydrocyclization (550°C), the selectivity to aromatization for these Pt-based catalysts has likely been significantly lowered relative to other competing reactions (hydrogenolysis, isomerization, C5 ring closure, etc.). Total combustible liquid yield, toluene yield, and toluene selectivity values are all low for these catalysts relative to the data shown previously for the Girdler G-41 catalyst in Table 2, although comparable to those obtained for the Cr/HTO:Si catalysts. However, since our experiments were performed with no H_2 in the feed, low catalyst activity coupled with significant and rapid catalyst deactivation was not surprising in the case of the Pt-based catalysts.

Since supported Pt catalysts are difficult to synthesize in highly dispersed forms which are stable at high temperature, another alternative is to disperse the Pt atoms within a given metal particle composed of an alloy between Pt and a second metal. Various explanations for the positive effect of alloying on catalyst performance have been postulated, including altering the size of Pt atom surface ensembles and electronic modification of the catalytic properties of Pt [90-92,100-102]. By forming Pt alloys, it is possible to achieve a large and controlled portion of isolated Pt atoms *via* dilution achieved in alloying techniques. Both Re and Ir are widely known as effective alloying additives to improve catalyst selectivity and deactivation resistance of Pt reforming catalysts [90,91]. A common industrial reforming catalyst composition consists of a Pt concentration ranging from 0.2 to 0.6 wt.%, promoted/alloyed with a few hundred to a few thousand ppm of various additives, such as Re, Ir, Sn, or Ge, all supported on a high surface area alumina support, whose acidity has been enhanced *via* chloride additions [69,103]. Of this range of compositions, active phases consisting of 0.3 wt.% Pt + 0.3 wt.% Re appear to be fairly popular [88,104,105]. Recently, Sn, although being an inactive single component catalyst, has been identified as an effective alloying additive for isobutane dehydrogenation catalysts [100-102].

Bournonville and Franck discussed the effect of alloying of Pt with a second metal on n-heptane dehydrocyclization at 470°C over a range H_2 pressures [69]. Alloying of Pt with a wide range of metals (Ir, Re, Sn, Ge, Pb, or Rh [M:Pt atomic ratio=1:3]) was found to affect catalyst activity relative to pure Pt catalysts and to shift the activity maximum to lower H_2 pressures (e.g.,

H_2:n-C_7H_{16} ~1-2). The Pt-Ir catalyst showed the highest activity, although the Pt-Rh and Pt-Re catalysts also exceeded the activity of the baseline 0.6 wt.% Pt catalyst at all H_2 pressures. It should be noted that, in general, the activity of the Pt-Re catalyst only marginally exceeded the activity of the Pt catalyst, except at low H_2 pressure (H_2:n-C_7H_{16} ~1), where larger differences in activity were observed. Interestingly, the Pt-Sn catalyst exceeded the activity of the baseline 0.6 wt.% Pt catalyst only at low H_2 pressure (H_2:n-C_7H_{16} ~ 1), not performing as well at higher H_2 pressures. For n-heptane dehydrocyclization at 495°C and 14.6 atm (5:1 H_2:n-C_7H_{16}), Carter, et. al [105] showed that Pt-Re (+ 0.9 wt.% Cl^-)/Al_2O_3 catalysts (1:1 Re:Pt, 0.3 wt.% Pt + 0.3 wt.% Re) outperformed 0.3 wt.% Pt (+ 0.9 wt.% Cl^-)/Al_2O_3 catalysts over a 40 h time-on-stream period with 0.5 ppm sulfur in the feed.

The comparison of the results of the different Pt-based/HTO:Si catalysts proved to be quite interesting. Although the Sn additive appeared to produce no improvement in total heptane conversion relative to the Pt/HTO:Si catalyst, combustible liquid and toluene yields, as well as toluene selectivity, improved by almost 50% relative to the values observed for the Pt/HTO:Si catalyst (see Table 3). In this regard, the Pt-Sn/HTO:Si catalyst also proved to be superior to the Pt-Re/HTO:Si catalyst. Liquid product analysis by gas chromatography showed that chromatograms representing the liquid products from the Pt/HTO:Si and Pt-Re/HTO:Si catalysts were significantly more complex (with respect to the large number of small peaks observed) relative to the results obtained for the Pt-Sn/HTO:Si catalyst. Time was not taken to identify all of the product liquid species since the activity of all of the Pt-based catalysts was low relative to the Girdler G-41 catalyst. However, these qualitative results are consistent with the increased toluene selectivity of the Pt-Sn/HTO:Si catalyst relative to the other Pt-based catalysts. One species in the liquid product that was quantified was pentanes. The Pt-Sn/HTO:Si catalyst produced a negligible amount of pentanes in the liquid products relative to the other Pt-based catalysts, indicating a higher selectivity toward dehydrocyclization (relative to hydrogenolysis). The higher activity for the Pt-Sn (~0.6:1 Sn:Pt atomic ratio)/HTO:Si catalyst is consistent with the better performance of Pt-Sn catalyst (1:3 Sn:Pt) at low H_2 pressure as described above [69]. Note that our experiments represented an extremely low H_2 pressure (H_2/n-heptane feed ratio = 0). The better performance of the Pt-Sn/HTO:Si catalyst might also be attributed to improved resistance to deactivation [90,91,100-102].

For heptane dehydrocyclization at milder reaction conditions (400°C, 1 atm H_2, pulse reactor), Tournayan, et al. [106] showed that increases in the Re content to an alumina-supported Pt catalyst (2% total Pt + Re) resulted in a steady decrease in specific catalyst activity (expressed as turnover frequency); selectivity changes involving decreased C5 ring closure/cyclization and increased hydrogenolysis activity were also noted with increasing Re content. On a mildly acidic alumina support, Garland, Baiker, and Wokaun found an optimum range of Re:Pt atomic ratio between 1:1 and 1:3 (0.5 wt.% total metal concentration) that enhanced both the selective dehydrocyclization of n-heptane to toluene and the selective dehydrogenation of methylcyclohexane to toluene [107]. This is consistent with a wealth of literature data which shows the high hydrogenolysis activity of supported Re catalysts, and increases in hydrogenolysis activity due to Re additions to supported Pt catalysts [90,108,109].

Relative to the Pt-Re compositional information described above, our Re:Pt atomic ratio was ~1:1. With respect to the data shown in Table 3, the Re additive appeared to offer a beneficial effect in terms of increased total heptane conversion as well as increased combustible liquid yield and toluene yield. This benefit is similar to the slightly higher catalyst activity observed for supported Pt-Re catalysts over the complete range of H_2 pressure relative to supported Pt catalysts in previous studies [69,105]. However, in conjunction with these improvements, a slightly higher concentration of alkanes was observed in the gas product, along with a small but significant quantity of pentanes in the liquid product. This is consistent with the increased hydrogenolysis activity associated with Re additions to supported Pt catalysts [90,107-109].

As an alternative to alloying, the intentional addition of S to Pt catalysts has been used to alter the structure of active sites (ensembles) or electronically modify the interaction between the active intermediate and the catalyst [110]. Recently, superior catalyst activity and deactivation resistance were obtained with a sulfided Pt/alumina catalyst relative to an unsulfided Pt-Re/alumina catalyst in methylcyclohexane dehydrogenation experiments in a catalytic membrane reactor [111]. A limited amount of adsorbed sulfur can also have beneficial effects for Pt-based alloy catalysts; the superior performance of supported Pt-Re catalysts for industrial reforming applications is consistent with this fact [103,105]. Alkali additions to monofunctional supported Pt or Pt-Sn catalysts have been shown to positively affect their activity, selectivity, and deactivation resistance in dehydrogenation and aromatization reactions [101,102,112,113]. Although not explored herein, the influence of alkali content in Pt-based/HTO:Si materials would be an interesting area to explore since the residual alkali content remaining in the as-prepared catalyst precursor can easily be controlled by the ion exchange solution chemistry variables. Recall that the original ion exchangeable titanate support is in alkali form (e.g. $NaTi_2O_5H$:0.4 SiO_2).

Because of the various sampling frequencies for the different catalysts, a time-on-stream value of 50 min was selected for comparison of the initial performance data of the respective Pt-based/HTO:Si catalysts shown in Table 3. However, all of the Pt-based/HTO:Si catalysts exhibited significant deactivation with increasing time-on-stream as illustrated by the data shown in Figure 16. Examination of the data in Figure 16 shows that the initial (30 min time-on-stream) activity (in terms of total heptane conversion) of both the Pt-Sn/HTO:Si and Pt-Re/HTO:Si catalysts significantly exceeded that of the Pt/HTO:Si catalyst. In terms of overall catalyst deactivation, the Pt-Sn/HTO:Si catalyst appeared to stabilize at ~20% total heptane conversion after 50 min time-on-stream, whereas the Pt/HTO:Si and Pt-Re/HTO:Si catalysts continued significant deactivation for time-on-stream values up to 100 min. As described above, it is possible that the lack of sulfur in the feed proved detrimental to the performance of the Pt/HTO:Si and Pt-Re/HTO:Si catalysts, while not having a significant effect on the Pt-Sn/HTO:Si catalyst. For all catalysts, the changes observed with increasing time-on-stream with respect to combustible liquid and toluene yields, as well as toluene selectivity, were found to mirror the trends observed for total heptane conversion, although the magnitude of the deactivation was less significant.

As in the case of the supported Cr catalysts, the Pt-based/HTO:Si catalysts were also evaluated after appropriate catalyst regeneration procedures, which included both an air treatment at 550°C for 10 min followed by a H_2 treatment at 550°C for 30 min. The performance of the Pt-based/HTO:Si catalysts was then evaluated after regeneration for comparison to the original data shown in both Table 3 and Figure 16. The total heptane conversion data as a function of time-on-stream for the Pt/HTO:Si, Pt-Re/HTO:Si, and Pt-Sn/HTO:Si catalysts after regeneration are shown in Figure 17.

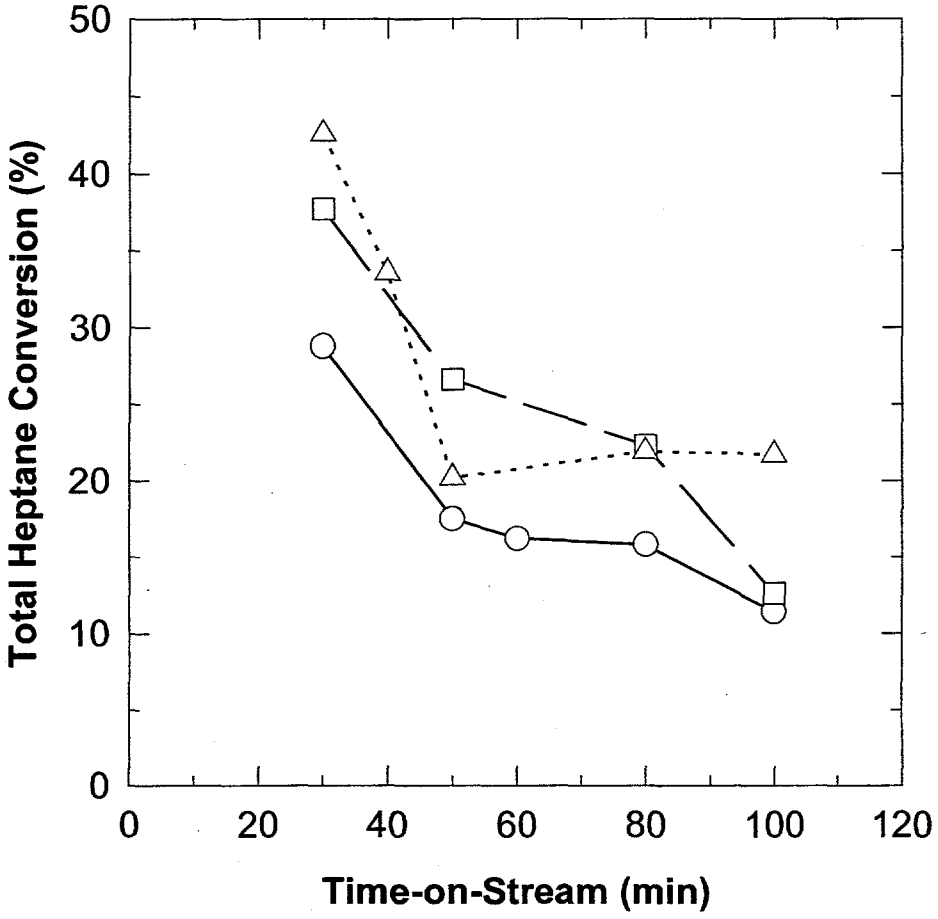

Figure 16. Initial data for total heptane conversion as a function of time-on-stream at 550°C and a nominal WHSV of 2 h^{-1} for the Pt-based/HTO:Si catalysts. The following catalysts are represented: Pt/HTO:Si (open circular symbols), Pt-Re/HTO:Si (open square symbols), and Pt-Sn/HTO:Si (open triangular symbols).

Significant changes in the performance of both the Pt-Re/HTO:Si and Pt-Sn/HTO:Si catalysts were observed after regeneration. As a reference, the initial performance of the Pt/HTO:Si catalyst is also included on Figure 17. Comparison of the results for the performance of the Pt/HTO:Si catalyst before and after regeneration shows that after regeneration, the activity of the Pt/HTO:Si catalyst returns to very close to the steady state activity observed after initial

deactivation (~15% total heptane conversion). The high activity observed for the Pt/HTO:Si catalyst in its initial clean state (~30% total heptane conversion) is not approached by the catalyst in its regenerated form. This might be due to incomplete removal of the carbonaceous deposits responsible for catalyst deactivation during the regeneration procedure or due to significant sintering of the Pt particles during the air regeneration step. While other studies have reported that careful passivation of supported metal catalysts is required prior to regeneration in oxidizing environments [46,87], our Pt-based/HTO:Si catalysts were exposed directly to air at elevated temperature (550°C) during the regeneration step. This may have resulted in a significant temperature excursion and metal particle sintering.

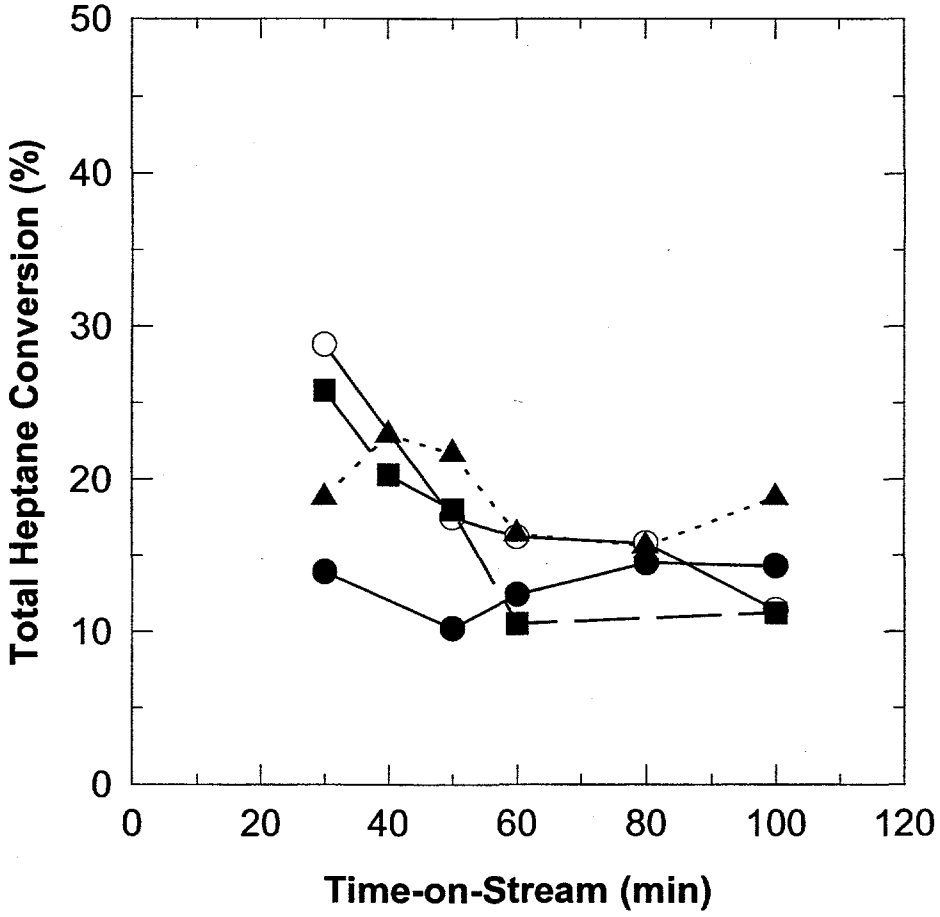

Figure 17. Data for total heptane conversion after one regeneration cycle as a function of time-on-stream at 550°C and a nominal WHSV of 2 h^{-1} for the Pt-based/HTO:Si catalysts. The following catalysts are represented: Pt/HTO:Si (filled circular symbols), Pt-Re/HTO:Si (filled square symbols), and Pt-Sn/HTO:Si (filled triangular symbols). As a reference, the open circular symbols represent the initial catalyst deactivation data for the Pt/HTO:Si catalyst (from Figure 16). The regeneration cycle consisted of a N_2 purge for 10 min at 550°C, followed by an air treatment for 10 min at 550°C, followed by a H_2 treatment at 550°C for 30 min.

In the case of the Pt-Re/HTO:Si and Pt-Sn/HTO:Si catalysts, activity after catalyst regeneration also did not approach the initial activity observed for the fresh catalysts (compare Figures 16 and 17). However, the initial activity of the regenerated Pt-Re/HTO:Si and Pt-Sn/HTO:Si catalysts was still significantly higher than that observed for the regenerated Pt/HTO:Si catalyst. The Pt-Re/HTO:Si catalyst again showed significant deactivation over the 100 min time-on-stream period after air regeneration, with the final total heptane conversion values approaching those observed for the regenerated Pt/HTO:Si catalyst in its final deactivated state (100 min time-on-stream). Similar to the fresh catalyst results, the Pt-Sn/HTO:Si catalyst appeared to perform better after regeneration than both the Pt-Re/HTO:Si and the Pt/HTO:Si catalysts. Less overall deactivation was observed for this catalyst, with total heptane conversion values ranging from 15 to 25% for time-on-stream values up to 100 min. In addition to the potential problems identified for the Pt/HTO:Si catalyst with respect to the regeneration procedure (incomplete hydrocarbon removal and sintering), the air oxidation procedure used for catalyst regeneration can have significant detrimental effects on the Pt-Re and Pt-Sn alloy particles. It would be expected that oxidation/reduction cycling of such alloys might ultimately result in segregation of the various alloying components, accompanied by the degradation or loss of catalyst activity or selectivity advantages [100,103,114].

Two final aspects of catalyst deactivation to be considered are the weight and surface area changes for the various supported Pt-based catalysts. In contrast to the Cr/HTO:Si samples described previously, all of the Pt-based/HTO:Si samples were calcined (600°C/2h/air) prior to testing, so these materials were expected to be very stable with respect to further weight loss and surface area reduction in the reactor environment. This allowed the effects of catalyst deactivation in terms of weight gain and surface area reduction to be directly measured. The initial surface areas of the calcined Pt-based/HTO:Si samples were ~135 m^2/g. Irrespective of composition, all of the samples showed a surface area reduction as a result of catalyst testing and had very similar surface area upon removal from the reactor (70-75 m^2/g). All Pt-based/HTO:Si samples showed a weight gain as a result of reactor testing, with weight gains ranging from 6-13 wt.%. Interestingly, the alloyed Pt compositions (Pt-Re and Pt-Sn) showed a significantly larger weight gain (11-13 wt.%) than the Pt/HTO:Si materials (6-8 wt.%). We find this interesting in light of the fact that the Pt-Sn/HTO:Si material apparently showed increased resistance to catalyst deactivation (see Figures 16 and 17).

The Pt-based/HTO:Si catalysts did show increased weight gain relative to the supported Cr catalysts evaluated. However, as mentioned previously, this is likely due to the selection of a common reaction temperature (550°C) that was more suitable for optimum performance of the supported Cr catalysts. This fact, combined with the lack of H_2 in the feed (H_2/n-heptane ratio = 0), would have significantly enhanced catalyst deactivation in the case of the Pt-based catalysts.

Summary

The efforts of this section were devoted to identifying high activity catalyst materials for use in n-heptane dehydrogenation/dehydrocyclization to toluene. In addition to evaluating a commercial catalyst benchmark (Girdler G-41 7.5 wt.% Cr/γ-Al_2O_3), HTO:Si-supported Cr and

Pt-based catalysts were also evaluated under identical conditions. The commercial Cr/γ-Al_2O_3 catalyst was clearly more active than the Cr/HTO:Si catalysts, and the inability to increase the Cr/HTO:Si catalyst activity through increases in Cr loading exacerbated the differences between these materials. Pt/HTO:Si, Pt-Re/HTO:Si, and Pt-Sn/HTO:Si catalysts were also evaluated for n-heptane dehydrogenation/dehydrocyclization activity at conditions similar to those of the supported Cr catalysts. Although several interesting trends were observed for the Pt-based/HTO:Si catalysts, because the reaction conditions were less optimum for supported Pt catalysts, significant deactivation with increasing time-on-stream was observed, and overall catalyst performance for these materials was not as good as the supported Cr catalysts. Continued investigation of Pt-based/HTO:Si catalysts under more favorable reactor operating conditions appears warranted, including the use of a relevant commercial Pt catalyst benchmark and the careful discrimination of thermal reactions and support acid site effects. Based on these overall bulk catalyst development results, the Girdler G-41 7.5 wt.% Cr/γ-Al_2O_3 catalyst was selected as the catalyst of choice for packed bed application in the catalytic membrane reactor experiments.

Chapter III. Catalytic Membrane Reactor Testing

Experimental

A baseline silica (A2** sol-derived) membrane was fabricated along the inside diameter of a 6 cm long asymmetric alumina membrane tube (1.0 cm OD and 0.7 cm ID) *via* dip coating (H_2O content > 10 ppm; stagnant atmosphere drying) as described in Chapter I. After calcination for 3 h at 550°C, surface derivatization of the baseline silica membrane was accomplished by dip coating the tube in a TEOS monomer solution (5 volume % TEOS in ethanol), and recalcining at 525°C for 3 h. The final membrane would therefore be considered a composite silica membrane since two dip coating applications, utilizing different sols, were performed. For catalytic membrane reactor testing, the membrane tube was packed with 1.34 g of a commercial 7.5 wt.% Cr/γ-Al_2O_3 catalyst (Girdler G-41) and heated to the reaction temperature (525 to 570°C) in flowing N_2. Pure gas permeation tests were conducted at 525°C with hydrogen and nitrogen in between the catalytic membrane reactor tests. The procedure used for the catalytic membrane reactor tests consisted of feeding n-heptane at weight hourly space velocities (WHSV) from 2-8 h^{-1} through the reactor for periods of 1.5 to 1.75 h and monitoring the effluent flow rate and hydrogen content of the residue and permeate gas streams. The partial pressure driving force required for hydrogen permeation was obtained by operating the permeate side under a reduced pressure of approximately 0.07 atm, with tube side pressures (P_t) of 1 to 4 atm. The effluent gas stream was analyzed on-line using a gas chromatograph equipped with a TCD. Four analyses of the effluent gas streams were made (generally 15-30 min apart) during each test period. Liquid residue from the reactor was collected in chilled condensers located on both the permeate and residue (retentate) lines. The liquid residue samples were collected at the end of each run (i.e., one liquid sample per run) and analyzed in a similar fashion to that described for the bulk catalyst

development activities in Chapter II. Following each run, the reactor was cooled to 450°C and the catalyst was reactivated by passing air through the reactor for a period of 1 h. This is in contrast to the bulk catalyst testing with the Girdler G-41 catalyst, where catalyst regeneration was performed at 550°C in air (see Chapter II).

The conventional packed bed reactor experiments described in Chapter II and these catalytic membrane reactor experiments were performed in different laboratories by separate personnel. This fact explains the subtle differences observed between the two data sets in terms of the experimental set-up and sampling protocol, on-line product gas analysis, product liquid collection, and regeneration procedures.

Results and Discussion

In terms of membrane performance and stability, the microporous silica membranes appear to be a promising candidate for this application. No condensed liquids were collected on the permeate side of the module which indicated that heptane and toluene are too large to permeate through the pores of the silica membrane. This fact alleviated the need to impart a catalytic functionality into the membrane to convert unreacted heptane as it passed through the membrane. However, small quantities of C1-C4 hydrocarbons were detected in the permeate stream at all catalytic membrane reactor operating conditions. The hydrogen concentration in the permeate stream was generally above 98 mole % so the membrane was able to effectively separate hydrogen from cracking products such as C1-C4 hydrocarbons. For reference, the mole % of H_2 in the combined permeate and retentate gas streams at all reaction conditions was always greater than 70%, and generally in the 85-95% range. Generalizing over all catalytic membrane reactor operating conditions, the order of decreasing hydrocarbon concentration in the permeate (or retentate) gas stream was $C_2H_6 > CH_4 > C_3H_8 > \Sigma C4$ species. Typical concentrations of these hydrocarbon species in the permeate stream were nearly always less than 0.5 mole %. Condensed liquid products detected included toluene, dimethylcyclopentanes, heptenes, pentanes, and benzene, in order of decreasing concentration, similar to the results obtained in the conventional packed bed reactor testing with the Girdler G-41 catalyst (see Chapter II). The apparent correlation between the gas and liquid product analyses indicated that hydrogenolysis reactions were occurring, with a higher preference of terminal bond scission relative to central bond scission in the case of these nonselective cracking reactions.

Table 4 shows the overall performance observed with the Girdler G-41 catalyst in the catalytic membrane reactor for the n-heptane dehydrogenation/dehydrocyclization reaction as a function of WHSV at a tube side pressure (P_t) of 1 atm, a reactor temperature of 550°C, and 60 min nominal time-on-stream. As described earlier in Chapter II, the theoretical toluene yield under the conditions of this study (550°C, 1 atm pressure) should be essentially 100 percent since there is no thermodynamic limitation on conversion. Because of this fact, the removal of product H_2 by the membrane would not be expected to provide a significant conversion benefit. However, it was still important to determine whether the change in reactor configuration had a significant effect on catalyst activity and selectivity. This comparison was possible over only a limited set of reactor operating conditions (WHSV and P_t).

In both cases, the total combustible liquid yield, toluene yield, and total heptane conversion data reported in Tables 2 and 4 for the two reactor configurations were calculated based on a similar liquid product analysis by gas chromatography using an FID. For the conventional packed bed reactor experiments, several liquid product samples were collected at discrete time intervals over the course of the run, allowing the evaluation of changes in the product liquid

Table 4. Catalytic membrane reactor results obtained with the Girdler G-41 7.5 wt.% Cr/γ-Al_2O_3 catalyst used in conjunction with a composite silica membrane for heptane dehydrogenation/dehydrocyclization. Catalyst activity and selectivity results obtained as a function of WHSV at a tube side pressure (P_t) = 1 atm, a reactor temperature of 550°C, and 60 min nominal time-on-stream.

WHSV (h^{-1})	H_2 Generation Rate/Heptane Feed Rate*	Total Heptane Conversion (%)[@,a]	Total Combustible Liquid Yield (%)[#,a]	Total Toluene Yield (%)[$,a]	H_2 Permeation Fraction[^]
2.94	1.16	36.5	23	17	0.79
2.96[+]	NA	44.0	28	19	NA
5.88	0.60	17.3	16.7	11	0.62
8.65	0.48	10.8	14	8.5	0.52

Notes:

* This measure of catalyst activity is based on the molar ratio of H_2 generated (as measured directly *via* a TCD used in conjunction with a gas chromatograph) to the heptane feed rate. A value of 4 would correspond to complete conversion of n-heptane to toluene *via* the reaction illustrated in Figure 12.

@, #, $ The definitions for these symbols are similar to those defined in Table 1.

[a] For catalytic membrane reactor experiments, these values were calculated as an average over the entire 80-105 min run since only a single liquid sample was collected over the duration of the experiment.

^ This measure of membrane performance represents the fraction of the product H_2 which permeates through the membrane and is based on the H_2 analysis of both the permeate and retentate streams.

+ Comparison data for conventional packed bed reactor operated under near identical conditions; data reproduced from Table 2. These values represent data collected over a 20 to 30 min time-on-stream interval at a WHSV of 2.96 h^{-1}, which directly followed a period of 20 min time-on-stream at a WHSV of 2.04 h^{-1}.

NA Not applicable or not measured.

composition with increasing time-on-stream. However, for the catalytic membrane reactor experiments, only a single product liquid sample was collected over the entire 80-105 min run. These results therefore represent an average of catalyst activity and selectivity over the entire run; this fact makes an evaluation of catalyst deactivation in the catalytic membrane reactor using the liquid product data impossible and also makes a comparison of the results for the two reactor configurations very difficult. Catalyst deactivation in the catalytic membrane reactor was monitored by evaluating catalyst activity *via* intermittent product gas stream analysis (for H_2 and C1-C4 hydrocarbons) using a TCD. Since this measurement was only performed in the case of the catalytic membrane reactor experiments, no direct link exists between this H_2 generation data and data measured in the case of the conventional packed bed reactor configuration.

Based on the above discussion, a limited comparison can be made between the results obtained in the catalytic membrane reactor at a WHSV value of 2.94 h^{-1} to those obtained at a similar WHSV value (2.96 h^{-1}) and operating pressure (1 atm) for the Girdler G-41 catalyst tested in the conventional packed bed reactor (see Table 2; this data is reproduced in Table 4 for ease of comparison). For these similar operating conditions, the total combustible liquid yield and the toluene yield for the catalytic membrane reactor are slightly less than those obtained in the case of the conventional packed bed reactor. However, given the fact that the product liquid analysis in the case of the catalytic membrane reactor sample represents an average over a long time interval, significant catalyst deactivation would be expected. In terms of the total heptane conversion, the decrease for the catalytic membrane reactor configuration relative to the conventional packed bed reactor is perhaps more significant, although the above statement regarding the sampling differences between the two reactor configurations applies in this case as well. Overall, the differences in catalyst activity determined for the two units are relatively small and easily within the limits of measurement error and extrapolation (in terms of catalyst deactivation effects). This provides a preliminary indication that the removal of H_2 *via* the microporous composite silica membrane does not significantly affect catalyst performance at these specific reaction conditions, although more careful experiments minimizing the sampling and analysis differences between the two reactor configurations would be necessary to provide more evidence to support this claim.

Table 4 also shows that an increase in space velocity results in a significant decrease in catalyst activity and product liquid selectivity. Similar to the discussion in Chapter II for tests in the conventional packed bed reactor, the total heptane conversion in the catalytic membrane reactor was roughly inversely proportional to the reactant flow rate (WHSV), validating the assumption of differential operating conditions. In addition to catalyst activity and selectivity, the performance of the membrane was evaluated in terms of the fraction of generated H_2 that was separated from the retentate *via* the microporous composite silica membrane. The lower WHSV values result in a larger fraction of the product H_2 permeating through the membrane, which is consistent with the longer residence time of the product gases in the catalytic membrane reactor. These overall results clearly indicate that even lower WHSV values are necessary to optimize catalytic membrane reactor performance.

Similar to the results obtained for the conventional packed bed reactor configuration, catalyst deactivation with time-on-stream was significant in the case of the catalytic membrane

reactor experiments. Hydrogen generation rates were observed to steadily decline over the 1.5 to 1.75 h test periods, which indicated significant deactivation problems with the commercial catalyst. Figure 18 shows the change in catalyst activity (in terms of H_2 generation rate/heptane feed rate) with increasing time-on-stream at a reaction temperature of 550°C and a tube side pressure (P_t) of 1 atm for WHSV values ranging from ~3-9 h^{-1}. Reinforcing the data shown in Table 4, it is clear that the highest H_2 generation rates were observed at the lowest WHSV value (2.94 h^{-1}); however, the rate of catalyst deactivation was also highest under these conditions,

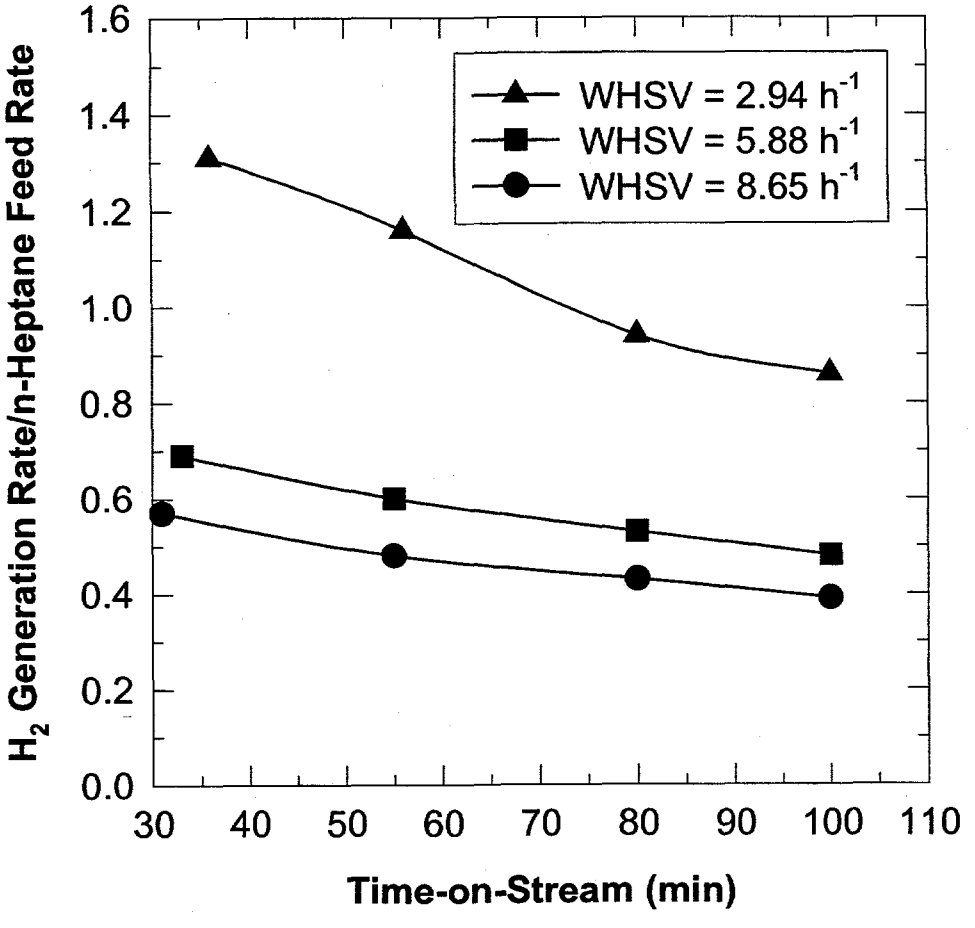

Figure 18. H_2 generation versus time-on-stream for the catalytic membrane reactor operated at various WHSV values with the Girdler G-41 7.5 wt.% Cr/γ-Al_2O_3 catalyst. For these experiments, the reactor temperature was 550°C and the tube side pressure (P_t) was 1 atm. See footnotes for Table 4 for a definition of the H_2 generation rate/heptane feed rate term.

especially in the range of 30-80 min time-on-stream. Over this time period, the H_2 generation rate/heptane feed rate decreased by ~28%. Under similar WHSV (2.96 h^{-1}) conditions, the catalyst deactivation observed with the conventional packed bed reactor was ~19% in terms of total heptane conversion over an initial 10-30 min time-on-stream period. Even this comparison is not perfect since there is no overlap in the time-on-stream intervals and different

measurements are involved. Additional discussion of catalyst deactivation observed with the conventional packed bed reactor configuration is detailed in Chapter II.

The effect of changing the tube side pressure (P_t) was examined in an effort to improve catalytic membrane reactor performance. These experiments were performed at a high WHSV value (~8 h^{-1}) with the results observed after ~50 min time-on-stream being shown in Table 5. The data show that the production of H_2 was optimized at P_t values ranging from 2-3 atm, with the percentage of hydrogen generated in the dehydrocyclization reaction that was recovered in the permeate stream being high as long as the tube side (reactor) pressure (P_t) was above 1 atm. The fraction of the H_2 product which permeated through the microporous composite silica membrane increased significantly with increasing P_t values due to the increased driving force for permeation/diffusion provided by the larger difference in pressure between the retentate and permeate sides of the membrane. Nonselective cracking reactions were enhanced at higher P_t values and reaction temperatures; under these conditions, the permeate stream contained a lower H_2 purity and higher C1-C4 hydrocarbon concentrations.

Table 5. Catalytic membrane reactor results obtained with the Girdler G-41 7.5 wt.% Cr/γ-Al_2O_3 catalyst used in conjunction with a microporous composite silica membrane for heptane dehydrogenation/dehydrocyclization. H_2 generation and permeation rates were obtained as a function of tube side pressure (P_t) at a WSHV of 8 h^{-1}, a reactor temperature of 550°C, and 60 min nominal time-on-stream.

Tube Side Pressure, P_t (atm.)	H_2 Generation Rate/Heptane Feed Rate	Overall H_2 Permeation Fraction
1.0	0.478	0.517
2.0	0.595	0.757
3.0	0.572	0.79
4.0*	0.438	0.83

Note:
* The data points for 4 atm. tube side pressure (P_t) represent a different reaction temperature (570°C).

The effect of other catalytic membrane reactor operating conditions on catalyst deactivation was also evaluated. In addition to the data shown in Table 5 regarding the effect of increasing tube side pressure (P_t), it was found that the rate of catalyst deactivation significantly increased with increasing reaction temperature. As might have been expected from the data observed for the conventional packed bed reactor (see Table 2), increases in reactor temperature (to 570°C) did not improve the product H_2 yield in the case of the catalytic membrane reactor configuration, even when a higher tube side pressure (P_t = 3 atm) was utilized. The use of a lower reaction temperature (525°C) was found to slightly decrease catalytic membrane reactor performance in terms of H_2 generation rate/heptane feed rate and H_2 permeation fraction. However, a higher

purity permeate stream and a lower rate of catalyst deactivation were observed under these conditions.

Another aspect critical to the operation of the catalytic membrane reactor is the performance of the membrane itself. To this extent, the microporous composite silica membrane was tested for a total of over 400 h at temperatures of 450°C and above. Figure 19 summarizes the results of H_2 and N_2 permeation tests conducted intermittently during this time period. The stability of this membrane was significantly better than that of similar membranes previously tested with a Pt/aluminosilicate catalyst for propane and isobutane dehydrogenation experiments, where H_2 permeance typically dropped by approximately 20-35% during 100 hour test periods [50]. In contrast, the H_2 permeance of the composite silica membrane tested in the heptane

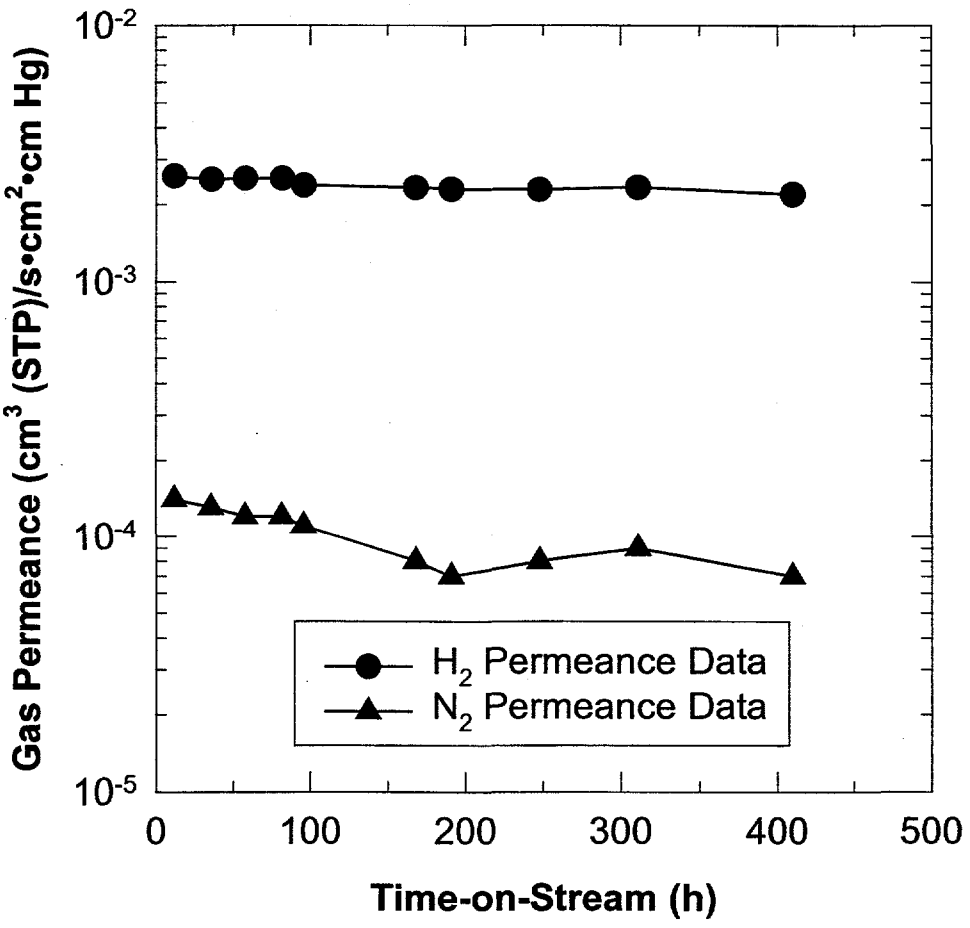

Figure 19. H_2 and N_2 permeance values at 525°C versus time-on-stream for microporous composite silica membrane used in heptane dehydrogenation/dehydrocyclization catalytic membrane reactor study.

dehydrogenation/dehydrocyclization experiments dropped by only 7.5% in the first 100 h of testing and 15% during the entire 400 h test period. As expected from the data shown in Figure 19, H_2/N_2 permselectivities (expressed as ideal separation factor, α_I) remained relatively constant (~20-30) over the course of the test period. Ioannides et al. have studied dense silica membranes

prepared by chemical vapor deposition in various catalytic membrane reactor applications, including isobutane dehydrogenation, dry reforming (CO_2 reforming of methane), and partial oxidation of methane [53,54]. They observed lower H_2 permeance for their membranes (0.3 $cm^3/(cm^2 \cdot min \cdot atm)$ or ~6.6 x 10^{-5} $cm^3/(cm^2 \cdot s \cdot cm\ Hg)$ at 600°C) and better H_2/N_2 permselectivities (200-300) than the sol-gel derived microporous silica membranes evaluated herein. Exposure to feeds containing H_2O decreased membrane permeance significantly due to densification of the silica membrane [54]. Although our baseline silica membrane materials would be susceptible to the same problems, it is hoped that the surface derivatization approaches used to tailor pore size in composite membrane materials might also impart increased stability in terms of resistance to densification in high temperature environments containing H_2O.

Even though it was difficult to compare the overall rate of catalyst deactivation in the catalytic membrane reactor with that observed in the conventional packed bed reactor, the important feature to note is that significant catalyst deactivation existed in either case. It might be expected that the removal of product H_2 would further increase the rate of catalyst deactivation in the case of the catalytic membrane reactor, since a much smaller fraction of the product H_2 remains available to prevent coking of the catalyst surface and subsequent deactivation relative to the conventional packed bed reactor. Even though many authors have demonstrated that equilibrium conversion limitations can be exceeded using *in situ* H_2 removal [12,14,19,47,50,52,54,55,61], catalyst deactivation problems related to this methodology have also been documented [12,14,19,50,52,53]. Ali et al. [47] have demonstrated improvements in conversion up to a factor of 4x (relative to equilibrium conversion values) for methylcyclohexane dehydrogenation to toluene in a packed bed reactor coupled with *in situ* H_2 removal using a composite Pd-Ag membrane. The largest improvements in conversion relative to the equilibrium values were observed at lower temperatures and higher pressures (up to 20 bars). This work and subsequent modeling efforts were performed using a pilot-scale unit under industrially relevant conditions.

Problems with catalyst deactivation due to *in situ* removal of H_2 from dehydrogenation/dehydrocyclization product streams have led several researchers to propose and test the use of *ex situ* H_2 removal in conjunction with conventional packed bed reactors. Both Rezac, et al. [51] and Ali, et al. [46,48] have demonstrated three stage reactor/membrane/reactor systems where *ex situ* removal of H_2 in the membrane only (no catalyst) stage was utilized to increase conversions beyond equilibrium limitations while minimizing catalyst deactivation. It is interesting to note that the former authors used a polymer-ceramic composite membrane to accomplish H_2 removal, while the latter authors used a Pd-Ag membrane. In principle, there is no reason that a microporous silica membrane could not be used with similar success in this membrane only *ex situ* H_2 removal stage. Matsuda, et al. [52] noted that for isobutane dehydrogenation in a catalytic membrane reactor, the performance of a Pt/Al_2O_3 catalyst deteriorated rapidly due to deactivation such that it was less active than a Cr/Al_2O_3 catalyst. Interestingly, $Pt\text{-}Sn/Al_2O_3$ catalysts performed significantly better in the catalytic membrane reactor than Pt/Al_2O_3 catalysts, presumably due to suppression of coke formation [52].

Of special note is the work published by Ali and Baiker [46] on a three stage reactor/membrane/reactor system (with *ex situ* H_2 removal in the membrane only stage) used for

n-heptane dehydrocyclization to toluene. Their work was performed using significantly different reaction conditions than our work; a Pt catalyst was utilized at reaction temperatures of 400-440°C, 17 bar total pressure, H_2/n-C_7H_{16} feed ratio ~2, and LHSV values ranging from 1.2-1.9 h^{-1}. The largest difference in overall conversion to toluene in their multistage system relative to equilibrium conversion values was observed at combinations of low LHSV values with low reaction temperature. These authors also observed significant catalyst deactivation with increasing time-on-stream, even though H_2 removal was not performed in direct conjunction with the catalyst bed. This deactivation was attributed to the low H_2/n-heptane feed ratios used for their experiments; Bournonville and Franck [69] recommend a H_2/n-heptane feed ratio range of 3-10 for supported Pt catalysts. As pointed out in Chapter II, this is a delicate balance since increasing the H_2 content of the feed beyond an optimum value lowers dehydrocyclization activity and increases the likelihood of other possible reaction pathways (e.g., hydrogenolysis and isomerization). Another problem is that the rate of n-heptane dehydrocyclization tends toward zero as the partial pressure of H_2 in the feed approaches zero; this explains why even ex-situ removal of H_2 using an interstage membrane separator can pose deactivation problems, particularly if the feed to the second packed bed reactor used in the three stage system of Ali and Baiker becomes H_2 deficient. Since all of our experiments utilized neat n-heptane feeds with no added H_2, this may explain the severe catalyst deactivation problems we experienced in both our conventional reactor and catalytic membrane reactor experiments. This overall finding suggests that the development of new catalysts which are less sensitive to the H_2 content of the feed and/or product stream (in the case of a multistage system) is an important area of future work.

Summary

These preliminary catalytic membrane reactor experiments were a successful proof of concept demonstration of the integration of the microporous composite silica membrane and conventional packed bed catalyst technologies. At industrially relevant space velocity values (WHSV = 3-8 h^{-1}), yields of the desired heptane dehydrocyclization products (toluene and H_2) were low. There are two main reasons for the low yields observed in our catalytic membrane reactor experiments: 1) catalyst activity was relatively low for this reaction; and 2) catalyst deactivation occurred rapidly due to the removal of product hydrogen by the membrane. In order to obtain higher yields with this catalyst, the reactor should be operated at lower space velocity or in another, more effective reactor configuration. Since there are no thermodynamic limitations on conversion in this application, the main purpose of the membrane is to separate H_2 from the other gas species and not to provide an equilibrium shift. Therefore, a more promising configuration would be to use a conventional reactor followed by a membrane separator. Since for this case there would be no hydrogen removal in direct conjunction with the catalyst bed, catalyst deactivation should be less of a problem in this "hybrid" reactor configuration. Other potential modifications to the current scheme might include increasing the partial pressure of H_2 to the reactor and/or recycling a portion of the product H_2 to help minimize catalyst deactivation. The inclusion of H_2 in the reactor feed and as well as higher pressure operating conditions in the catalytic membrane reactor would more closely simulate industrial reforming conditions and also impose equilibrium constraints for which the catalytic membrane reactor unit could provide additional benefits.

These initial benchmarking experiments demonstrated that more active, selective, and deactivation-resistant catalysts are required to increase liquid product yield and H_2 production. Initial membrane performance was better than expected, especially in terms of membrane selectivity to H_2 and overall membrane stability at high temperature reaction conditions over extended periods of time. The current limitations imposed by relatively low catalyst activity and significant catalyst deactivation are important challenges which must be overcome before it would be practical to produce a prototype catalytic membrane reactor to demonstrate the practicality of our H_2 generation scheme.

Overall Summary and Recommendations

Membrane development studies determined that it was not possible to replicate the "thermal cut-off" behavior observed for baseline (solvent-templated) silica membranes. It was possible to integrate ion-exchangeable HTO films into the structure of composite microporous ceramic membranes, although the catalytic advantage of this integration was determined to be minimal. However, additional fundamental studies related to microporous ceramic membranes led to the development of surfactant-templated silica membranes with ordered micro/mesoporosity. Upon subsequent surface derivatization, the resulting composite membranes yield both higher flux and permselectivity to H_2 than previous composite membrane options. These new composite membrane materials offer great promise for both membrane separation and catalytic membrane reactor applications.

Relative to the n-heptane dehydrogenation/dehydrocyclization activity of the commercial benchmark catalyst (Girdler G-41 Cr/γ-Al_2O_3), the performance of Cr/HTO:Si catalysts is poor due to a fundamental limitation of the Cr/HTO:Si technology. Although the results obtained with the Pt-based/HTO:Si catalysts were inferior to the commercial Cr/γ-Al_2O_3 catalyst, these preliminary results should be considered promising since it is clear that the chosen reactor operating conditions were more optimum for supported Cr catalysts. Continued investigation of Pt-based/HTO:Si catalysts under more favorable reactor operating conditions appears warranted, including the use of a relevant commercial Pt catalyst benchmark and the careful discrimination of thermal reactions and support acid site effects. Regardless of the supported catalyst used in conjunction with a membrane separation system, it is clear that significant improvements in the activity, selectivity, and deactivation resistance of these catalyst materials are required to enable the utilization of catalytic membrane reactor units for chemical production.

The preliminary catalytic membrane reactor experiments were a successful proof of concept demonstration of the integration of the microporous ceramic membrane and conventional packed bed catalyst technologies. Further work with new optimized catalyst formulations that have higher activity, selectivity, and deactivation resistance is clearly justified. This work should also incorporate improvements to the microporous ceramic membrane materials where possible,

such as the new composite silica membrane materials produced *via* the surfactant-templating + surface derivatization route. Finally, in an effort to boost overall catalytic membrane reactor system performance, design changes which allow for *ex situ* H_2 removal, the inclusion of H_2 in the feed, and/or the recycle of product H_2 should be evaluated.

References

1. S. G. Chalk, "Is There a Continuing Role for the Federal Government in Fuel Cell R&D for Transportation?," 1998 Fuel Cell Seminar, Book of Abstracts, sponsored by the Fuel Cell Seminar Organizing Committee, Palm Springs, CA, November, 1998, pp. 222-225.

2. C. Borroni-Bird, "Automotive Fuel Cell Requirements," Preprints of the Annual Automotive Technology Development Customers' Coordination Meeting, Vol. 1, U.S. Department of Energy, Washington, DC, October, 1996.

3. P. B. Davis, "DOE Automotive Fuel Cell Development Program," Preprints of the Annual Automotive Technology Development Customers' Coordination Meeting, Vol. 1, U.S. Department of Energy, Washington, DC, October, 1996.

4. R. Espino, "Fuels Processing for PEM Fuel Cells – Fuels Industry Perspective," Preprints of the Annual Automotive Technology Development Customers' Coordination Meeting, PNGV Workshop on Fuel Processing for Proton Exchange Membrane (PEM) Fuel Cells, U.S. Department of Energy, Washington, DC, October, 1995.

5. R. A. Kost, "Hybrid Propulsion Systems Development," Preprints of the Annual Automotive Technology Development Customers' Coordination Meeting, Vol. 1, U.S. Department of Energy, Washington, DC, October, 1996.

6. E. H. Wakefield, History of Electric Automobile: Hybrid Electric Vehicles, SAE Publications, Warrendale, PA, 1998.

7. R. Kumar, "Overview of Fuel Processing Options for Polymer Electrolyte Fuel Cell Systems," Preprints of the Annual Automotive Technology Development Customers' Coordination Meeting, PNGV Workshop on Fuel Processing for Proton Exchange Membrane (PEM) Fuel Cells, U.S. Department of Energy, Washington, DC, October, 1995.

8. L. F. Brown, "A Survey of Processes for Producing Hydrogen Fuel from Different Sources for Automotive-Propulsion Fuel Cells," Los Alamos National Laboratory Report, LA-13112-MS, Los Alamos, NM, March, 1996.

9. T. J. Flynn, R. M. Privette, M. A. Perna, K.E. Kneidel, D. L. King, and M. Cooper, "Compact Fuel Processor for Fuel Cell-Powered Vehicles," SAE Paper No. 1999-01-0536.

10. J. C. Amphlett, K. A. M. Creber, J. M. Davis, R. F. Mann, B. A. Peppley, and D. M. Stokes, "Hydrogen Production by Steam Reforming of Methanol for Polymer Electrolyte Fuel Cells," Int. J. Hydrogen Energy, 19[2] (1994), pp. 131-137.

11. J. C. Amphlett, R. F. Mann, B. A. Peppley, P. R. Roberge, A. Rodrigues, and J. P. Salvador, "Simulation of a 250 kW Diesel Fuel Processor/PEM Fuel Cell System," J. Power Sources, 71 (1998), pp. 179-184.

12. H. P. Hsieh, "Inorganic Membrane Reactors," Cat. Rev. - Sci. Eng., 33 (1&2) 1991, pp. 1-70.

13. J. N. Armor, "Challenges in Membrane Catalysis," CHEMTECH, September, 1992, pp. 557-563.

14. G. Saracco, G. F. Versteeg, and V. P. M. van Swaaij, "Current Hurdles to the Success of High Temperature Membrane Reactors," J. Membr. Sci., 95 (1994), pp. 105-123.

15. G. Saracco and V. Specchia, "Catalytic Inorganic Membrane Reactors: Present Experience and Future Opportunities," Catal. Rev.-Sci. Eng., 36[2] (1994), pp. 305-384.

16. J. N. Armor, "Membrane Catalysis: Where is it Now, What Needs to be Done?," Cat. Today, 25 (1995), pp. 199-207.

17. J. Shu, B. P. A. Grandjean, A. Van Neste, and S. Kaliaguine, "Catalytic Palladium-Based Membrane Reactors: A Review," Canad. J. Chem. Eng., 69 (1991), pp. 1036-1060.

18. J. L. Falconer, R. D. Noble, and D. P. Sperry, "Catalytic Membrane Reactors," in The Handbook of Membrane Separations, S. A. Stern and R. D. Noble, Eds., Marcel Dekker, New York (1993).

19. E. Kikuchi, "Hydrogen-Permselective Membrane Reactors," CATTECH, March, 1997, pp. 67-74.

20. S. R. Vatcha, F. Trifiro, and F. Cavani, "Oxidative Dehydrogenation and Alternate Dehydrogenation Processes," Catalytica Studies Division Report, Mountain View, CA, 1993.

21. D. C. Grenoble and M. M. Estadt, "The Chemistry and Catalysis of the Water-Gas Shift Reaction. 1. The Kinetics Over Supported Metal Catalysts," J. Catal., 67 (1981), pp. 90-102.

22. M. J. Kahlich, H. A. Gasteiger, and R. J. Behm, "Kinetics of the Selective CO Oxidation in H_2 Rich Gas on Pt/Al_2O_3," J. Catal., 171 (1997), pp. 93-105.

23. R. F. Mann, J. C. Amphlett, and B. A. Peppley, "A Fuel Conditioning System for a Methanol Fuelled PEM Fuel Cell Power Generator," in Frontiers Science Series, Number 7, T. Ohta and T. Homma, Eds., Universal Academy Press, 1993, pp. 613-618.

24. J. C. Amphlett, R. F. Mann, and B. A. Peppley, "On Board Hydrogen Purification for Steam Reformation/PEM Fuel Cell Vehicle Power Plants," Int. J. Hydrogen Energy, 21[8] (1996), pp. 673-678.

25. S. Gottesfeld, "Fuel Purity Requirements for PEM Fuel Cells," Preprints of the Annual Automotive Technology Development Customers' Coordination Meeting, PNGV Workshop on Fuel Processing for Proton Exchange Membrane (PEM) Fuel Cells, U.S. Department of Energy, Washington, DC, October, 1995.

26. J. L. Humphrey, "Separation Processes: Playing a Critical Role," Chem. Eng. Progr., October, 1995, pp. 31-41.

27. W. J. Koros, "Membranes: Learning a Lesson from Nature," Chem. Eng. Progr., October, 1995, pp. 68-81.

28. W. J. Koros and G. K. Fleming, "Membrane-Based Gas Separations," J. Membr. Sci., 83 (1993), p. 1.

29. R. Prasad, F. Notaro, and D. R. Thompson, "Evolution of Membranes in Commercial Air Separation," J. Membr. Sci., 94 (1994), pp. 225-248.

30. S. A. Stern, "Polymers for Gas Separations: The Next Decade," J. Membr. Sci., 94 (1994), pp. 1-65.

31. J. Robeson, "Correlation of Separation Factor Versus Permeability for Polymeric Membranes," J. Membr. Sci., 62 (1991), pp. 165-185.

32. K. Keizer, R. J. R. Uhlhorn, V. T. Zaspalis, and A. J. Burggraaf, "Transport and Related (Gas and Vapour) Separation in Ceramic Membranes," in Proceedings of the 2nd International Congress on Inorganic Membranes, A. J. Burggraaf, J. Charpin, and L. Cot, Eds., Trans Tech Publications, Zurich (1991), pp. 143-154.

33. R. J. R. Uhlhorn, K. Keizer, and A. J. Burggraaf, "Gas-Transport and Separation with Ceramic Membranes. 1. Multilayer Diffusion and Capillary Condensation," J. Membr. Sci., 66 (1992), pp. 271-287.

34. C. J. Brinker, S. Wallace, N. K. Raman, R. Sehgal, J. Samuel, and S. M. Contakes, "Sol-Gel Processing of Amorphous Nanoporous Silicas: Thin Films and Bulk," in Access in Nanoporous Materials, T. J. Pinnavaia, and M. F. Thorpe, eds., Plenum Press, New York (1995), p. 123.

35. C. J. Brinker, R. Sehgal, N. K. Raman, S. K. Prakesh, and L. Delattre, "Sol-Gel Strategies for Controlled Porosity Ceramic Materials: Thin Film and Bulk," Mat. Res. Soc. Symp. Proc., Vol. 368 (1995), p. 329.

36. C. J. Brinker, R. Sehgal, S. L. Hietala, R. Deshpande, D. M. Smith, D. Loy, and C. S. Ashley, "Sol-Gel Strategies for Controlled Porosity Inorganic Materials," J. Membr. Sci., 94 (1994), p. 85.

37. L. C. Klein and N. Giszpenc, "Sol-Gel Processing for Gas Separation Membranes," Bull. Am. Ceram. Soc., 69[11] (1990), pp. 1821-1830.

38. R. S. A. DeLange, J. H. A. Hekkink, K. Keizer, A. J. Burggraaf, "Formation and Characterization of Supported Microporous Ceramic Membranes Prepared by Sol-Gel Modification Techniques," J. Membr. Sci., 99 (1995), pp. 57-75.

39. R. S. A. DeLange, J. H. A. Hekkink, K. Keizer, A. J. Burggraaf, "Permeation and Separation Studies on Microporous Sol-Gel Modified Ceramic Membranes," Microporous Mater., 4[2-3] (1995), pp. 169-186.

40. T. Bein, "Synthesis and Applications of Molecular Sieve Layers and Membranes," Chem. Mater., 8 (1996), pp. 1636-1653.

41. Y. Yan and T. Bein, "Zeolite Thin Films with Tunable Molecular Sieve Function," J. Am. Chem. Soc., 117 (1995), pp. 9990-9994.

42. Z. A. E. P. Vroon, K. Keizer, A. J. Burggraaf, and H. Verweij, "Preparation and Characterization of Thin Zeolite MFI Membranes on Porous Supports," J. Membr. Sci., 144 (1998), pp. 65-76.

43. Z. A. E. P. Vroon, K. Keizer, M. J. Gilde, H. Verweij, and A. J. Burggraaf, "Transport Properties of Alkanes Through Ceramic Thin Zeolite MFI Membranes," J. Membr. Sci., 113 (1996), pp. 293-300.

44. A. J. Burggraaf, Z. A. E. P. Vroon, K. Keizer, and H. Verweij, "Permeation of Single Gases in Thin Zeolite MFI Membranes," J. Membr. Sci., 144 (1998), pp. 77-86.

45. K. Keizer, A. J. Burggraaf, Z. A. E. P. Vroon, and H. Verweij, "Two Component Permeation Through Thin Zeolite MFI Membranes," J. Membr. Sci., 147 (1998), pp. 159-172.

46. J. K. Ali and A. Baiker, "n-Heptane Reforming in a System of Reactors-Interstage Membrane to Separate Hydrogen," Appl. Catal. A, 140 (1996), pp. 99-110.

47. J. K. Ali, E. J. Newson, and D. W. T. Rippin, "Exceeding Equilibrium Conversion with a Catalytic Membrane Reactor for the Dehydrogenation of Methylcyclohexane," Chem. Eng. Sci., 49(13) (1994), pp. 2129-2134.

48. J. K. Ali, D. W. T. Rippin, and A. Baiker, "Improving Methylcyclohexane Dehydrogenation with Ex-Situ Hydrogen Separation in a Reactor-Interstaged Membrane System," Ind. Eng. Chem. Res., 34 (1995), pp. 2940-2948.

49. J. K. Ali, E. J. Newson, and D. W. T. Rippin, "Deactivation and Regeneration of Pg-Ag Membranes for Dehydrogenation Reactions," J. Membr. Sci., 89 (1994), pp. 171-184.

50. J. P. Collins, R. W. Schwartz, R. Sehgal, T. L. Ward, C. J. Brinker, G. P. Hagen, and C. A. Udovich, "Catalytic Dehydrogenation of Propane in Hydrogen Permselective Membrane Reactors," Ind. Eng. Chem. Res., 35 (1996), pp. 4398-4405.

51. M. E. Rezac, W. J. Koros, and S. J. Miller, "Membrane-Assisted Dehydrogenation of Normal Butane," Ind. Eng. Chem. Res., 34 (1995), pp. 862-868.

52. T. Matsuda, I. Koike, N. Kubo, and E. Kikuchi, "Dehydrogenation of Isobutane to Isobutene in a Palladium Membrane Reactor," Appl. Catal. A., 96 (1993), p. 3.

53. T. Ioannides and G. R. Gavalas, "Catalytic Isobutane Dehydrogenation in a Dense Silica Membrane Reactor," J. Membr. Sci., 77 (1993), pp. 207-220.

54. T. Ioannides and X. E. Verykios, "Application of a Dense Silica Membrane Reactor in the Reactions of Dry Reforming and Partial Oxidation of Methane," Catal. Lett., 36 (1996), pp. 165-169.

55. E. Gobina and R. Hughes, "Reaction Assisted Hydrogen Transport During Catalytic Dehydrogenation in a Membrane Reactor," Appl. Catal. A., 137 (1996), pp. 119-127.

56. B. A. Raich and H. C. Foley, "Supra-Equilibrium Conversion in Palladium Membrane Reactors: Kinetic Sensitivity and Time Dependence," Appl. Catal. A., 129 (1995), pp. 167-188.

57. N. Itoh, "A Membrane Reactor Using Palladium," AIChE J., 33[9] (1987), pp. 1576-1578.

58. N. Itoh, Y. Shindo, K. Haraya, and T. Hakuta, "A Membrane Reactor Using Microporous Glass for Shifting-Equilibrium of Cyclohexane Dehydrogenation," J. Chem. Eng. Jpn., 21[4] (1988), pp. 399-404.

59. Y. L. Becker, A. G. Dixon, W. R. Moser, and Y.H. Ma, "Modelling of Ethylbenzene Dehydrogenation in a Catalytic Membrane Reactor," J. Membr. Sci., 77 (1993), pp. 233-244.

60. A. Giroir-Fendler, J. Peureux, H. Mozzanega, and J.-A. Dalmon, "Characterization of a Zeolite Membrane for Catalytic Membrane Reactor Application," Stud. Surf. Sci. Catal., 101 (1996), pp. 127-136.

61. A. M. Champagnie, T. T. Tsotsis, R. G. Minet, and I. A. Webster, "A High Temperature Catalytic Membrane Reactor for Ethane Dehydrogenation," Chem. Eng. Sci., 45[8] (1990), pp. 2423-2429.

62. R. Soria, "Overview on Industrial Membranes," Catal. Today, 25 (1995), pp. 285-290.

63. A. G. Sault and E. P. Boespflug, "Selective Dehydrogenation over Hydrous Titanium Oxide-Supported Catalysts," Sandia National Laboratories, SAND96-1889, Albuquerque, 1996.

64. A. G. Sault and E. P. Boespflug, "Selective Dehydrogenation of Ethylbenzene over Hydrous Titanium Oxide-Supported Iron Catalysts," submitted to Ind. Eng. Chem. Res. Dev.

65. R. G. Dosch and L. I. McLaughlin, "Hydrous Metal Oxide-Supported Catalysts: Part III. Development of NiMoHMO Catalysts," Sandia National Laboratories, SAND92-0388, Albuquerque, March, 1992.

66. S. E. Lott, T. J. Gardner, L. I. McLaughlin, and J. B. Oelfke, "Evaluation of Hydrous Titanium Oxide-Supported NiMo Catalysts for Pyrene Hydrogenation and Upgrading Coal-Derived Liquids," Fuel, 75[12] (1996), pp. 1457-1466.

67. R. Sehgal, "Microporous Gas Separation Membranes: Fundamentals, Preparation, and Characterization," Ph. D. Dissertation, University of New Mexico, 1996.

68. J. Speight, The Chemistry and Technology of Petroleum, Second Edition, Marcel Dekker, New York (1991).

69. J.-P. Bournonville and J.-P. Franck, in Hydrogen Effects in Catalysis: Fundamentals and Practical Applications, Z. Paal and P. G. Menon, eds., Marcel Dekker, New York, 1988, pp. 653-677.

70. C. J. Brinker, K.D. Keefer, D.W. Schaefer, and C. S. Ashley, "Sol-Gel Transition in Simple Silicates," J. Non-Cryst. Sol., 48 (1982), pp.47-64.

71. C. J. Brinker, A. J. Hurd, P. R. Schunk, G. C. Frye, and C. S. Ashley, "Review of Sol-Gel Thin Film Formation," J. Non-Cryst. Solids, 147-148 (1992), pp. 424-436.

72. H. P. Stephens and R. G. Dosch, "Catalyst Preparation via Hydrous Metal Oxide Ion-Exchangers," Stud. Surf. Sci. Catal., 31 (1987), pp. 271-283.

73. R. G. Dosch, H. P. Stephens, F. V. Stohl, B. C. Bunker, and C. H. F. Peden, "Hydrous Metal Oxide-Supported Catalysts: Part I. Preparation Chemistry and Physical and Chemical Properties," Sandia National Laboratories, SAND89-2399, Albuquerque, February, 1990.

74. Y. Lu, R. Ganguli, C. A. Drewien, M. T. Anderson, C. J. Brinker, W. Gong, Y. Guo, H. Soyez, B. Dunn, M. H. Huang, and J. I. Zink, "Continuous Formation of Supported Cubic and Hexagonal Mesoporous Films by Sol-Gel Dip Coating," Nature, 389 [25] (1997), p. 364.

75. G. C. Frye, A. J. Ricco, S. J. Martin, and C. J. Brinker, "Characterization of the Surface Area and Porosity of Sol-Gel Films Using SAW Devices," Mat. Res. Soc. Symp. Proc., 121 (1988), pp. 349-354.

76. C. J. Brinker, N. K. Raman, M. N. Logan, R. Sehgal, R. A. Assink, D.-W. Hua, T. L. Ward, "Structure-Property Relationships in Thin-Films and Membranes," J. Sol-Gel Sci. Technol., 4 (1995), pp. 117-133.

77. C. J. Brinker, T. L. Ward, R. Sehgal, N. K. Raman, S. L. Hietala, D. M. Smith, D.-W. Hua, and T. J. Headley, "Ultramicroporous Silica-Based Supported Inorganic Membranes," J. Membr. Sci., 77 (1993), pp. 165-179.

78. N. K. Raman, M. T. Anderson, and C. J. Brinker, "Template-Based Approaches to the Preparation of Amorphous, Nanoporous Silicas," Chem. Mater., 8 (1996), p. 1682.

79. G. Cao, Y. Lu, L. Delattre, C. J. Brinker, and G. P. Lopez, "Amorphous Silica Molecular Sieving Membranes by Sol-Gel Processing," Adv. Mater., 8 [7] (1996), p. 588.

80. N. K. Raman and C. J. Brinker, "Organic Template Approach to Molecular-Sieving Silica Membranes," J. Membr. Sci., 105 (1995), pp. 273-279.

81. Tsai, C.-Y., C. J. Brinker, "Silica Gas Separation Membranes Prepared with Surfactant-Templated Sublayers," Proceedings of the Fifth International Conference on Inorganic Membranes, Nagoya, Japan (1998), pp.180-183.

82. L. S. White, T. A. Blinka, H. A. Kloczewski, and I. S. Wang, "Properties of a Polyimide Gas Separation Membrane in Natural Gas Streams," J. Membr. Sci, 103 (1995), pp. 73-82.

83. R. G. Dosch, H. P. Stephens, and F. V. Stohl, "Hydrous Metal Oxide-Supported Catalysts: Part II. Catalytic Properties and Applications," Sandia National Laboratories, SAND89-2400, Albuquerque, February, 1990.

84. S. E. Lott, T. J. Gardner, and L. I. McLaughlin, "Screening of Hydrous Metal Oxide-Supported Catalysts for NOx Reduction by Hydrocarbons in Oxidizing Environments," Sandia National Laboratories, SAND96-2267, Albuquerque, September, 1996.

85. A. G. Sault, E. P. Boespflug, A. Martino, and J. Kawola, "Selective Dehydrogenation of Propane Over Novel Catalytic Materials," Sandia Report, SAND 98-0435, Albuquerque, February, 1998.

86. H. Pines, The Chemistry of Catalytic Hydrocarbon Conversions, Academic Press, New York, 1981, Ch. 4, Dehydrogenation and Cyclodehydrogenation (Aromatization), pp. 185-212.

87. H. Steiner, "Catalytic Cyclization and Aromatization of Hydrocarbons," in Catalysis, Vol. 4, P. H. Emmett, ed., Rheinhold, New York, 1956, pp. 529-560.

88. G. C. Bond, Heterogeneous Catalysis: Principles and Applications, Second Edition, Clarendon Press, Oxford, 1987.

89. Z. Paal, "Hydrogen Effects in Skeletal Reactions of Hydrocarbons over Metal Catalysts," in Hydrogen Effects in Catalysis: Fundamentals and Practical Applications, Marcel Dekker, Inc., New York, 1988, pp. 449-497.

90. V. Ponec, "Catalysis by Alloys in Hydrocarbon Reactions," Adv. Catal., 32 (1983), pp. 149-214.

91. J. H. Sinfelt, Bimetallic Catalysts: Discoveries, Concepts, and Applications, John Wiley and Sons, New York, 1983.

92. E. H. Broekhoven and V. Ponec, "Mechanism of Skeletal Reactions of Hydrocarbon on Metals," Prog. Surf. Sci., 19(4) (1985), pp. 351-400.

93. United Catalysts, Inc., Products Catalog.

94. K. K. Kearby, "Catalytic Dehydrogenation," in Catalysis, P. H. Emmett, ed., Vol. 3, Reinhold, New York (1955), pp. 453-491.

95. E. F. G. Herrington and E. K. Rideal, "On the Catalytic Cyclization of Aliphatic Hydrocarbons. I.," Proc. Roy. Soc. A., 184 (1945), pp. 434-446.

96. C. F. Baes, Jr., and R. E. Mesmer, The Hydrolysis of Cations, John Wiley and Sons, New York, 1976.

97. S. M. Davis, F. Zaera, and G. A. Samorjai, "Surface Structure and Temperature Dependence of n-Hexane Skeletal Rearrangement Reactions Catalyzed Over Platinum Single Crystal Surfaces: Marked Structure Sensitivity of Aromatization," J. Catal., 85 (1984), pp. 206-223.

98. R. W. Joyner, B. Lang, and G. A. Samorjai, "Low Pressure Studies of Dehydrocyclization of n-Heptane on Platinum Crystal Surfaces Using Mass Spectrometry, Auger Electron Spectroscopy, and Low Energy Electron Diffraction," J. Catal., 27 (1972), pp. 405-415.

99. W. D. Gillespie, R. K. Herz, E. E. Petersen, and G. A. Samorjai, "The Structure Sensitivity of n-Heptane Dehydrocyclization and Hydrogenolysis Catalyzed by Platinum Single Crystals at Atmospheric Pressure," J. Catal., 70 (1981), pp. 147-159.

100. S. M. Stagg, C. A. Querini, W. E. Alvarez, and D. E. Resasco, "Isobutane Dehydrogenation on Pt-Sn/SiO_2 Catalysts: Effect of Preparation Variables and Regeneration Treatments," J. Catal., 168 (1997), pp. 75-94.

101. J. M. Hill, R. D. Cortright, and J. A. Dumesic, "Silica- and L-Zeolite-Supported Pt, Pt/Sn, and Pt/Sn/K Catalysts for Isobutane Dehydrogenation," Appl. Catal. A, 168 (1998), pp. 9-21.

102. R. D. Cortright and J. A. Dumesic, "L-Zeolite-Supported Platinum and Platinum/Tin Catalysts for Isobutane Dehydrogenation," Appl. Catal. A, 129 (1995), pp. 101-115.

103. R. Prestvik, K. Moljord, K. Grande, and A. Holmen, "The Influence of Pretreatment on the Metal Function of a Commercial Pt-Re/Al_2O_3 Reforming Catalyst," 174 (1998), pp. 119-129.

104. R. Prestvik, B. Tøtdal, C. E. Lyman, and Anders Holmen, "Bimetallic Particle Formation in Pt-Re/Al_2O_3 Reforming Catalysts Revealed by Energy Dispersive X-Ray Spectrometry in the Analytical Electron Microscope," J. Catal., 176 (1998), pp. 246-252.

105. J. L. Carter, G. B. McVicker, W. Weissman, W. S. Kmak, and J. H. Sinfelt, "Bimetallic Catalysts: Application in Catalytic Reforming," Appl. Catal. 3 (1882), pp. 327-346.

106. L. Tournayan, R. Bacaud, H. Charcosset, and G. LeClercq, "Conversion of n-Heptane on Platinum-Rhenium/Alumina Catalysts in Hydrogen at 400°C," J. Chem. Res., Miniprint (1978), pp. 3582-3595.

107. M. Garland, A. Baiker, and A. Wokaun, "Alumina-Supported Platinum-Rhenium Dehydrogenation Catalysts: Influence of Metal Ratio and Precursors on Catalytic Behavior," Ind. Eng. Chem. Res., 30 (1991), pp. 440-447.

108. D. C. Grenoble, "The Chemistry and Catalysis of the Toluene Hydrodealkylation Reaction. I. The Specific Activities and Selectivities of Group VIIB and Group VIII Metals Supported on Alumina., J. Catal., 56 (1979), pp. 32-39.

109. C. Betizeau, G. Leclercq, R. Maurel, C. Bolivar, H. Charcosset, R. Frety, and L. Tournayan, "Platinum-Rhenium-Alumina Catalysts. III. Catalytic Properties," J. Catal., 45 (1979), pp. 179-188.

110. Z. Paal, M. Muhler, and K. Matusek, "Sulfided Pt Catalysts: Monitoring Surface Chemical State and Catalytic Properties in n-Hexane Reactions," J. Catal., 175 (1998), pp. 245-251.

111. J. K. Ali and D. W. T. Rippin, "Comparing Mono- and Bimetallic Noble Metal Catalysts in a Catalytic Membrane Reactor for Methylcyclohexane Dehydrogenation," Ind. Eng. Chem. Res., 34 (1995), pp. 772-729.

112. T. Fukunaga and V. Ponec, "On the Role of Additives to Platinum Catalysts for Reforming Reactions," Appl. Catal. A, 154 (1997), pp. 207-219.

113. B. E. Spiewiak, P. Levin, R. D. Cortright and J. A. Dumesic, "Microcalorimetric and Reaction Studies of Alkali Metals on Pt Powder and Pt/SiO_2, and $Pt/Sn/SiO_2$ Catalysts," J. Phys. Chem., 100 (1996), pp. 17260-17265.

114. T. P. Chojnacki and L. D. Schmidt, "Microstructures of Pt-Sn and Rh-Sn Particles on SiO_2," J. Catal., 129 (1991), pp. 473-485.

DISTRIBUTION:

2 John P. Collins
Amoco Research Center
Mail Code E-1E
150 West Warrenville Rd.
Napierville, IL 60563

1	MS 0188	LDRD Office, 4001
10	MS 0710	Timothy J. Gardner, 1841
1	MS 0710	Linda I. McLaughlin, 1841
1	MS 0710	James E. Miller, 1841
1	MS 0710	Alan P. Sylwester, 1845
2	MS 1349	C. Jeffrey Brinker, 1831
2	MS 1349	Allen G. Sault, 1841
2	MS 1349	C.Y. Tsai, UNM
1	MS 1349	Alan J. Hurd, 1841
2	MS 1452	Elaine P. Boespflug, 1552
1	MS 9018	Central Technical Files, 8940-2
2	MS 0899	Technical Library, 4916
1	MS 0619	Review and Approval Desk, 15102 For DOE/OSTI